12-16-2020

Simulation of Photoelectron Spectra of Small Organic Molecules

MD Mahbub
Georgia State University, mahbub.md009@gmail.com

SIMULATION OF PHOTOELECTRON SPECTRA OF SMALL ORGANIC MOLECULES

by

MD MAHBUB

Under the Direction of Samer Gozem, PhD

ABSTRACT

Photoelectron spectroscopy (PES) is a technique that uses photons in the energy range above a molecules' ionization threshold to probes the electronic structure of that molecule. Interpretation of the PES spectra often requires support from theory and computer modeling. This thesis focuses on the calculation of the total photoionization cross sections, which requires accurate wave functions of the initial and final states of the system. While the initial and final state of the molecular system can be represented using a single orbital, the final state also requires a description of the free electron wave function. At this moment, no black-box method exists that can be applied in a fast and systematic way to obtain accurate photoelectron spectra of polyatomic molecular systems. We will present a series of benchmarks using approximate and easy to implement treatments of the photoelectron wave functions, where we will compare computed and experimental photoionization spectra.

INDEX WORDS: Photoelectron Spectroscopy, Cross Section, Dyson Orbital, Wave Function, Electronic Structure, Computational Chemistry.

SIMULATION OF PHOTOELECTRON SPECTRA OF SMALL ORGANIC MOLECULES

by

MD MAHBUB

A Thesis Submitted in Partial Fulfillment of the Requirements for the Degree of

Master of Science

in the College of Arts and Sciences

Georgia State University

2020

SIMULATION OF PHOTOELECTRON SPECTRA OF SMALL ORGANIC MOLECULES

by

MD MAHBUB

Committee Chair: Samer Gozem

Committee: Shahab A. Shamsi

Markus Germann

Electronic Version Approved:

Office of Graduate Services

College of Arts and Sciences

Georgia State University

December 2020

DEDICATION

I would like to dedicate my work to my wife Khadija Ashraf, who is/was always with me 8500 miles away from my home, who never blamed my shortfall, never asked anything beyond my limitations.

ACKNOWLEDGEMENTS

Dr. Samer Gozem, my supervisor and mentor, who has helped me in multiple ways to reach this stage. I have learnt from him that giving limitless dedication is possible while learning. I can proudly say thanks to all of my group members, Yoelvis, Mohammad Pabel Kabir, Rebecca, Nicolas, Nykki, Nabi, Jorge and many others. I highly appreciate my respected thesis committee Dr. Shahab A. Shamsi and Dr. Markus Germann for paying interest and managing their schedule to guide me to get to my goal of completing my M.S. thesis work.

TABLE OF CONTENTS

LIST OF FIGURES

LIST OF ABBREVIATIONS

Photoelectron Spectroscopy	PES
Coulomb Wave	CW
Plane Wave	PW
Ultraviolet Photoelectron spectroscopy	UPS
X-Ray Photoelectron Spectroscopy	XPS
Ionization Energy	IE
Augmented Correlation-Consistent Polarized Valence Triple Zeta	aug-cc-pVTZ

1 INTRODUCTION

Photoelectron spectroscopy (PES) measures the binding energies of electrons in molecules. In combination with theoretical calculations, it provides a detailed insight into the electronic structure of molecules. This chapter introduces basic aspects of the experimental technique and methods to model PES computationally. The chapter also provides several former examples where studies of small organic molecules have been particularly fruitful with our proposed computational methods

1.1 Background

PES is a powerful spectroscopic method where electromagnetic radiation in the energy range above the ionization threshold of an atom or molecule is used to probe its electronic structure.[1-3] More specifically, PES experiments typically measure the kinetic energy and count of electrons emitted upon ionization of the system by high-energy monochromatic photons.[4] The graphical plot of the photoelectron spectrum is the number of electrons that are emitted from the energy level versus the kinetic energy. Another, related, type of spectroscopy, often yielding what is known as photoionization or photodetachment spectra, scans the count of electrons emitted as a function of the energy of the ionizing radiation used.[5] Such experiments typically discuss how the electron count, or photoionization/photodetachment cross-section, varies with the energy of light. Both PES and photoionization/photodetachment spectra can be used to analyze the energetics and distribution of electrons and nuclei in molecules.

Understanding ionization energy (IE) is a prerequisite for understanding PES. In general, the minimum amount of energy required to remove an electron from the ground state, the state of lowest energy, of one atom or molecule in the gas phase is called the ionization energy. Sometimes the term ionization potential is used in place of ionization energies, which denotes

the potential difference, in electron volt (eV), through which an electron must be moved so that it can overcome its potential energy.[4] Typically, IE refers to the ionization of an electron from the highest occupied molecular orbital (HOMO) of the system. Ionization energies differ based on the number of electrons of atoms or molecular orbitals and their shielding effect. The n^{th} ionization energy is the energy required to remove n^{th} electron after (n-1) have been removed from the atoms or molecules. Below is the chemical representation for the 1^{st} ionization of a neutral molecule:

$$X + Energy \rightarrow X^+ + e^- \quad \ldots\ldots\ldots\ldots\ldots\ldots\ldots\ldots\ldots\ldots (1)$$

Binding energies (BEs) more generally refer to the removal of an electron from any orbital of an atom or molecule. i.e., while IE specifically refers to ionization from the HOMO, BE is more commonly used to also refer to ionization from other orbitals such as the HOMO-1, HOMO-2, etc. Generally, electrons reside in atoms or molecules in orbitals, with each orbital having a maximum capacity of two electrons due to the Pauli exclusion principle. BE changes for individual atoms or molecules based on which orbital the ejected electron originally resided in. For example, the outermost electrons (valence electrons) are farthest from the nucleus on average and more shielded than the inner (core) electrons, and therefore have a lower BE.

Upon irradiating an atom or molecule with photons having more energy than its BE, an electron is ejected that stores the extra energy (energy above the BE) as kinetic energy, as shown in the following equation:

$$E_{Photon} = BE + E_{Electron(Kinetic)} \quad \ldots\ldots\ldots\ldots\ldots\ldots\ldots\ldots\ldots\ldots (2)$$

If the photon energy is known, the measured kinetic energies of the electrons can be used to determine the BEs of the atoms/molecules from which they originated. The electron count can

also be used to determine the photoionization and photodetachment cross section of the molecule from the pressure and temperature of the system.[6]

Figure 1.1.1 describes the PES spectrum of molecular hydrogen. The molecular orbitals of hydrogen are formed by the combination of two 1s atomic orbitals to generate one bonding $1\sigma_g$ orbital and one antibonding $1\sigma_u$ orbital. The PES has single band that corresponds to the ionization of an electron from the $1\sigma_g$ bonding orbital. The multiple peaks observed in the PES spectrum (red peaks) are due to ionization to different vibrational energy levels of the ionized state (vibronic structure).[7]

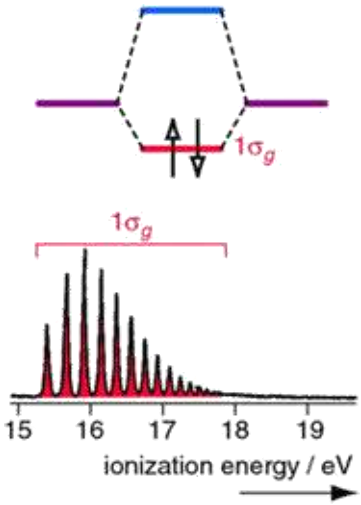

Figure 1.1.1 Photoelectron spectrum molecular hydrogen. Adapted from reference 7.[7]

Another example, shown in Figure 1.1.2, describes the PES of molecular nitrogen. The PES is slightly more complex since nitrogen has multiple molecular orbitals compare to molecular hydrogen. Five valence molecular orbitals are occupied (including two degenerate $1\pi_u$ orbitals). The UV photoelectron spectrum of N_2, has three bands corresponding to $3\sigma_g$, $1\pi_u$, and $2\sigma_u$ occupied molecular orbitals. Both $3\sigma_g$ and $2\sigma_u$ are weakly bonding and antibonding. The $1\sigma_g$, $1\sigma_u$, and $2\sigma_g$ orbitals are not included in this example since their BE appears at a

higher energy than scales used in the plot.[7] Note that both Figs. 1.1.1 and 1.1.2 are schematic figures meant to illustrate the principles of PES. The real PES spectra are often complicated by additional peaks arising due to autoionizing resonance states.

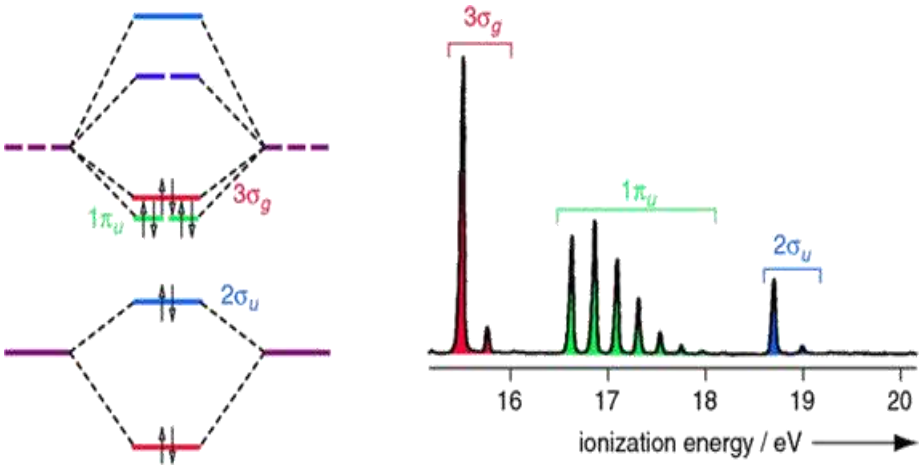

Figure 1.1.2 Photoelectron spectrum of molecular nitrogen. Adapted from reference 7.[7]

Photoelectron spectroscopy relies on the more familiar photoelectric effect, the original phenomenon presented by Albert Einstein in 1905. This experiment is widely viewed as one of the experiments that played a major role in the development of quantum mechanics. In Einstein's experiment, electrons on a metal surface are exposed to ionizing radiation above the ionization threshold (in the case of metal surfaces this is called the work function). Regardless of the intensity of light used, electrons get ejected from the atoms of the metal surfaces only when the frequency of light is above the ionization threshold. At that point, the number of photoelectrons ejected is directly proportional to the intensity of the incident light for a given metal and given frequency of incident radiation. This was an indication that light behaves in some ways like a particle rather than a wave and led to the wave-particle understand we currently have. Increasing the frequency will ultimately increase the kinetic energy of the emitted electron. A pictorial representation of the photoelectric effect is shown in Figure 1.1.3.

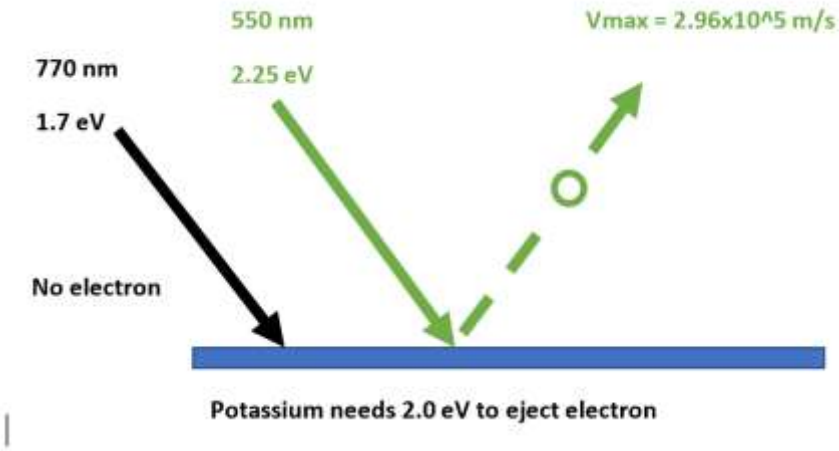

Figure 1.1.3 The Photoelectric effect, an electron is ejected when a surface is irradiated with light having more energy than the work function (ionization potential) of the metal.

The difference between the photoelectric effect and photoelectron spectroscopy is that the first one is more often used to the photoemission phenomenon itself while the latter is more often to discuss the experimental technique.

The potential application of PES depends on the energy regime used. Generally, there are two types of PES, based on the light sources; Ultraviolet photoelectron spectroscopy (UPS) and X-Ray photoelectron spectroscopy (XPS). UPS studies are mainly focused on the electronic structure of solids, adsorbed molecules on metals, and determination of bonding, antibonding, and nonbonding molecular orbitals. XPS studies are usually focused[8] on the elemental composition, empirical formula determination, chemical state, electronic state, binding energy[9], and layer thickness in the upper portion of the surfaces. Both UPS and XPS have widespread applications in fields such as astrochemistry, environmental, atmospheric, and combustion chemistry[10], and other fields where scientists are interested in the gas-phase reactivity of molecules.

Computational methods for the determination of IEs, or more generally BEs, are relatively well developed and tested.[11,12] However, there are far fewer studies addressing the simulation of the energy dependence of the probability of ejecting the electron (i.e., the electron count, or photoionization cross-section, as a function of ionizing radiation energy). The accurate simulation of both the IEs/BEs and the photoionization cross sections is very useful to supplement PES experiments, for instance in the ultrafast detection and quantification of transient intermediates in the gas phase.[13] Researchers often also employ PES to categorize bonding in molecules,[14] as shown in the N_2 example shown earlier.

While PES is not a new method, it has been receiving a lot of recent attention because the experiments are becoming easier to perform due to more powerful and accessible high-energy lasers. However, the interpretation of experimental results is not straightforward and often requires theory and computer modeling to support the data analysis. Calculation of photoionization and photodetachment cross-sections require accurate wave functions of the initial and final states of the system. Essential information of these states of the system can be found from special types of orbitals called Dyson orbitals, which can be calculated accurately from existing electronic structure methods. Additionally, the final state of the electron requires a description of its wave function. At this moment, no black box method exists that can be applied in a fast and systematic way to obtain accurate photoelectron spectra of polyatomic molecular systems. Existing computational approaches are either not quantitative or require time-consuming methods and expertise. We are working on the modeling the free-electron wave function to calculate the total cross-sections of the systems that are in quantitative or semi-quantitative agreement with experimental spectra.

1.2 Experimental and Computational Overview of Photoelectron Spectroscopy:

1.2.1 Experimental Overview:

Experimentally, as discussed in the background, PES is categorized into one of those two main techniques, UPS or XPS, depending on the sources of the incident light[8]. UPS is mainly focused on ejecting electrons from valence orbitals, whereas XPS is more often used to eject core electrons. In some applications, XPS is also called Electron Spectroscopy of Chemical Analysis (ESCA) when used for elemental analysis.

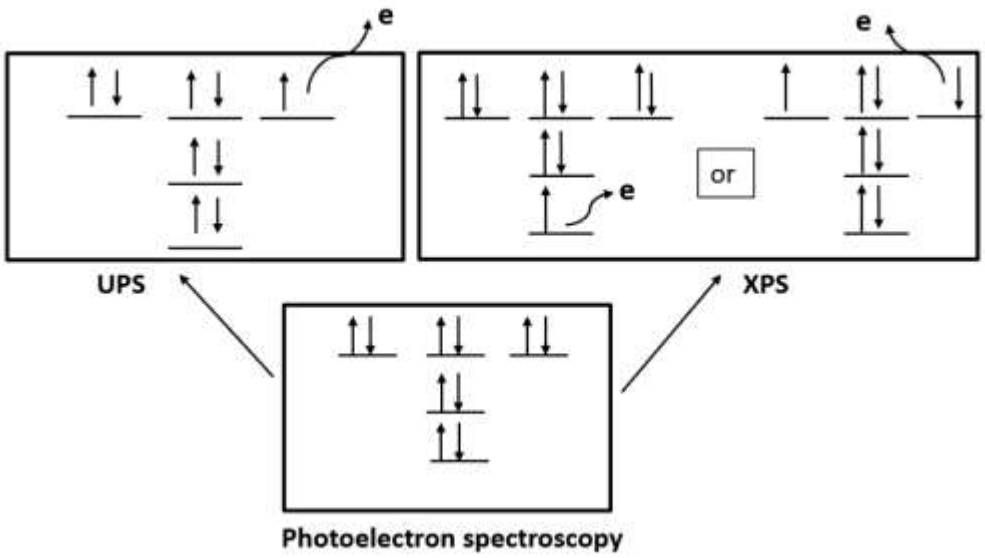

Figure 1.2.1 Electron ejection from Neon (or F^-), either from valence orbitals (e.g., 2p) by UPS or either valence or core orbitals (e.g., 1s) by XPS.

UPS uses ultraviolet radiation (< 41eV)[15], which is typically enough for the ionization of valence shell electrons. UPS experiments are typically performed using a helium (He) discharge lamp.[16,17] For XPS, the source is high energy X-rays which have energies of about 100 eV to 124 keV. XPS experiments often employ metal discharge lamps[18], which can be used to eject electrons from the core of atomic orbitals and valence orbitals as well (Figure 1.2.1).

Both UPS and XPS have three main basic components in their experimental setup:

1. Radiation sources (e.g., He discharge lamp for UPS, metal discharge lamp for XPS)

2. Analyzer; (Used for dispersing the electrons based on kinetic energy and measure the flux of emitted electron of given energy)
3. Ultra-High Vacuum Environment; (to avoid the interference of gas-phase collisions and analyze the photo-emitted electrons)

1.2.2 Computational Overview:

As mentioned in the background section, there are multiple methods for the simulation of binding energies with relatively high accuracy.[19,20] We will focus in this thesis on the calculation of photoionization and photodetachment cross sections. These calculations require accurate wave functions of the initial and final state of the system, as well as the wave function of the ejected electron. It is possible to compute all three wave functions at the same time using methods that mix bound and continuum basis functions,[21] or methods that simulate the continuum using very diffuse basis functions.[22,23] However, such methods are not easy to implement or apply. Instead, it is possible to compute the system wave functions independently of the photoelectron wave function. All information about the system that is relevant to ionization can be abridged into a one-electron function called the Dyson orbial.[24] Dyson orbitals can currently be computed accurately using correlated electronic structure methods.[25]

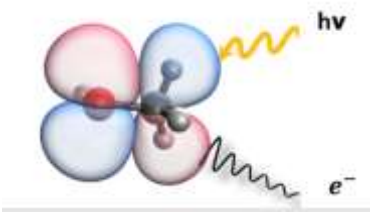

Figure 1.2.2 Dyson Orbital of methanol.

Figure 1.2.2 above showing the Dyson orbital of methanol, which is computed from Equation-of-Motion-Couple-Cluster Single and Double electron (EOM-CCSD) wave

functions.[26-28] These orbitals are computed in Q-Chem,[29] an electronic structure software package that prints out the coefficients of the orbital in an atomic orbital (AO) basis set, as well as the norm of the Dyson orbital.[30,31]

To calculate the total photoionization/photodetachment cross sections, we start with calculation of the photoionization/photodetachment differential cross-section, which is expressed by $\frac{d\sigma}{d\Omega_k}$:[3,32]

$$\frac{d\sigma}{d\Omega_k} = \frac{4\pi^2 kE}{c} |D_k^{IF}(\theta, \phi)|^2 \quad \text{..... (3)}$$

Here, k is the magnitude of the photoelectron wave vector $\boldsymbol{k}$. E is the ionization energy of the system, and c is the speed of light.

Information about electronic states of the system is included in the dipole matrix element, **(D_k^{IF})**, which can be computed as follows;

$$D_k^{IF} = \left\langle \Psi_I^N \left| \mathbf{u} \cdot \mathbf{r} \right| \Psi_F^{N-1} \cdot \Psi_k^{el} \right\rangle \text{..... (4)}$$

r is the dipole moment operator, and **u** is a unit vector in the direction of the polarization of light. By assuming strong orthogonality conditions, a simplified version of equation (3) will include Dyson orbital that has necessary information of the system before and after ionization,

$$D_k^{IF} = \left\langle \phi^d | r_u | \Psi_k^{el} \right\rangle \text{..... (5)}$$

Here, Ψ_k^{el} is the ejected electron wave function, and Φ_{IF}^d is the Dyson orbital which abridges the relevant information from the initial (N -electron) and final (N-1- electron) states:

$$\phi_{\mathrm{IF}}^{\mathrm{d}}(1) = \sqrt{N} \int \Psi_{\mathrm{I}}^N(1, \ldots, n) \Psi_{\mathrm{F}}^{N-1}(2, \ldots, n) d2 \ldots dn \quad \text{.....(6)}$$

Once the differential cross section is computed using equation (3), the total cross section can be computed by integrating this equation over all solid angles (A solid angle is a 3D angular

volume that is defined analogously to the definition of a plane angle in two dimensions[33]). This is the approach that is used in this thesis, and the calculation of the cross sections given a set of Dyson orbitals is performed in a stand-along program named *ezDyson*.[32]

The main difficulty in this approach is the need to use a reasonable photoelectron wave function, Ψ_k^{el}, that accounts for the interaction of the ejected electron with the remainder of the system. This is explained in more detail in the next section (Section 1.3). Also needed for the simulation of the photoelectron spectra are experimental details such as the laser polarization, ionization energy, molecular orientation (or averaging approach), and the range of electron kinetic energy.

To obtain a quantitative agreement between computed and experimental photoelectron spectra, it is often necessary to include the effect of molecular vibrations on the computed spectra (e.g., as shown in Figure 1.1.2 for N_2 in the background section). This requires the calculation of Franck-Condon factors, which are the overlaps between ground states and excited states.

1.3 Previous Work and Motivation:

Accurate molecular photoionization cross-sections can be computed with a modified central potential model that accounts for the non-spherical charge distribution of the core by adjusting the charge in the center of the expansion[2]. There are several methods used for the simulation of photoelectron spectra.

Instead, the approach that we will focus on in this thesis is derived from a simpler model, which employs accurate descriptions of the molecular system before and after ionization (represented using a Dyson orbital) but uses a simple treatment of the photoelectron wave function. Though Dyson orbitals give all the electronic information about the initial and final

state, the difficult part in this approach is properly model the ejected photoelectron wave function. Oana *et al.* have proposed a simpler model of photoionization (strong orthogonality and single-center expansion) employing Dyson orbitals computed using high-level electronic structure methods, where the photoelectron wave function treated as a Plane wave (PW) (Figure 1.3.1). Gozem *et al.*[34] then extended this method to testing a Coulomb wave (CW) (Figure 1.3.1) approach, instead of a plane wave, for treating the photoelectron wave function in the case of photoionization of neutral atoms and molecules.

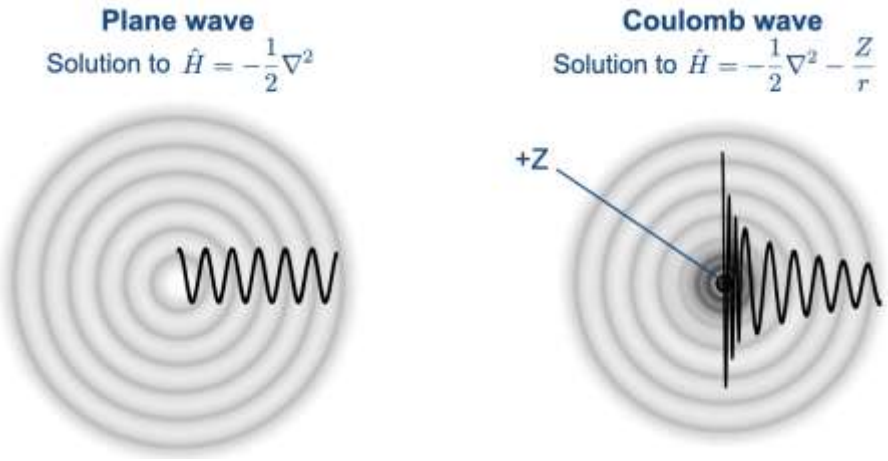

Figure 1.3.1 Schematic representation of Plane wave and Coulomb wave.

Gozem *et al.*[34] found that for small anions, a PW treatment provides a good description of the photodetachment spectra. For neutral atoms or molecules with one heavy atom, on the other hand, a CW treatment accounting for a +1 charge of the ionized core gives a better description of the photoionization (Figure 1.3.2). In fact, for small systems like Helium and Neon for which accurate experimental photoionization spectra are available, computations using a CW description of the photoelectron gave an excellent agreement with experiments. This is because the PW approximation assumes no electrostatic interaction between the ejected photoelectron

and the remaining core, while the CW the ionized core is simply treated as a point charge that exerts an electrostatic interaction on the ejected electron. Note that the computational approach here only models direct photoionization and does not account for resonance states such as those observed in the He experimental spectrum in Figure 1.3.2 at around 60 eV.[35,36]

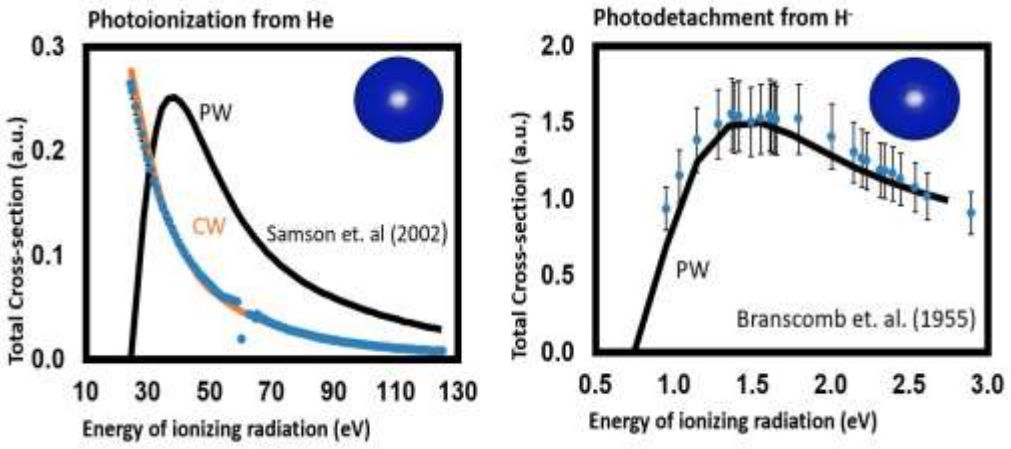

Figure 1.3.2 Photoionization (left) and Photodetachment (right) cross-section using Coulomb wave and plane wave treatment of the wave function. Photoionization from the He shows that Plane-wave approximation is not a good fit with the experimental cross-section, while a Coulomb wave gives an excellent agreement with the experiment. On the other hand, photodetachment from Hydrogen anion plane wave is working well. Figures are generated using computational results of Gozem et. al[34], and experimental results from Samson et al.[37] (left) and Branscomb et al.[38] (right).

For larger systems, both the plane and coulomb wave approximations (using a full +1 charge) usually fail to give a good agreement with the experimental cross-sections. Instead, often the best agreement with experiments could only be achieved by using a CW with partial (effective) charge smaller than unity[34].

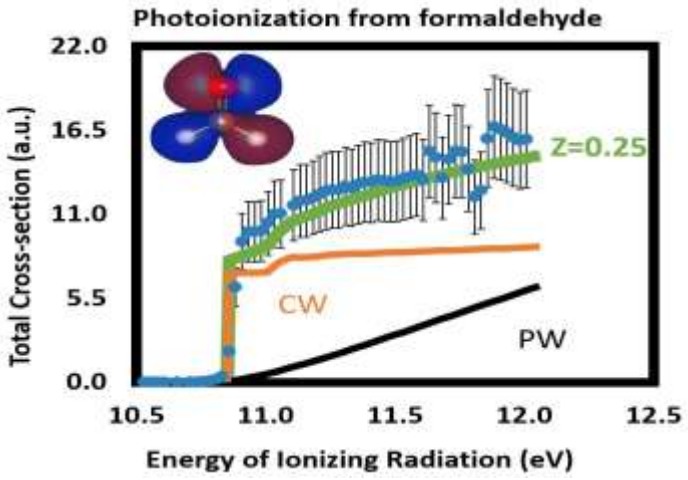

Figure 1.3.3 Absolute cross-sections for formaldehyde photoionization. The experimental cross-sections[39] are shown in blue dots, the computed values[34] for the plane wave (PW) are shown in the black line, and the orange line indicates the coulomb wave (CW). The green line shows the coulomb wave partial effective charge (Z= 0.25). The error bars are shown in the figure is in the range of +/- 20% from the experimental values. Figures are generated using computational results of Gozem et. al[34], and experimental results from Dodson et al.[39]

This effective charge can be considered to account for screening effects at the centroid of the Dyson Orbital that serves as the origin of the spherical wave expansion. Figure 1.3.3 shows experimental and computed photoelectron spectra for a sample system, formaldehyde. In this case, the CW gives a step-function-like shape, whereas the calculated based on the PW results in a gradually rising. The sharp rise of the threshold energy is typically a feature of the CW model and the gradual rise of energy is the feature of the PW model. However, using the value of Z = 0.25 leads to a much better agreement with the experimental results.

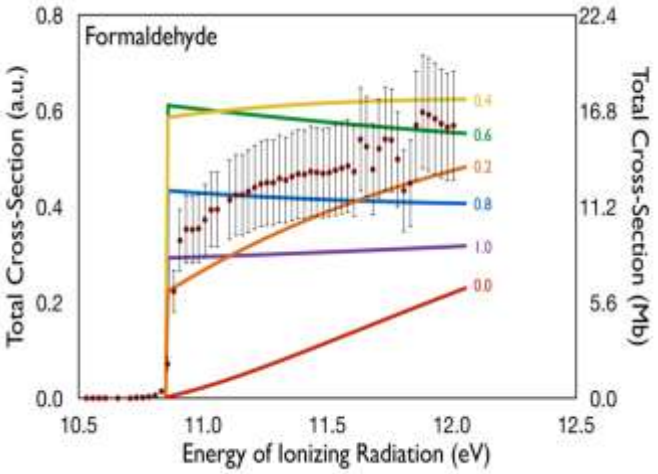

Figure 1.3.4 Cross sections (without Franck Condon factor) using different values of Z.[34]

The approach by Gozem *et al.* is not predictive unless there is an approach to predict the effective charge for each molecule. The authors have shown that the absolute cross sections are in some cases strongly modulated by the value of the partial effective charge used (See Figure 1.3.4 for formaldehyde with different Z values). The authors suggest a variational approach for obtaining the effective charge. Note that the dependence of the total cross section on the energy and effective charge can be understood by plotting the shape of the photoelectron radial function, $R_l(kr)$, (see Figure 1.3.5) and its overlap with $r\phi_{IF}^{d}$. In the figure, Y-axis represents the radial function and the X-axis represents the distance from the center of expansion in units of the Bohr radius. The bohr radius, a physical constant, is equal to the most probable distance between the nucleus and the electron in a hydrogen atom in its ground state (non-relativistic and with an infinitely heavy proton).[40]

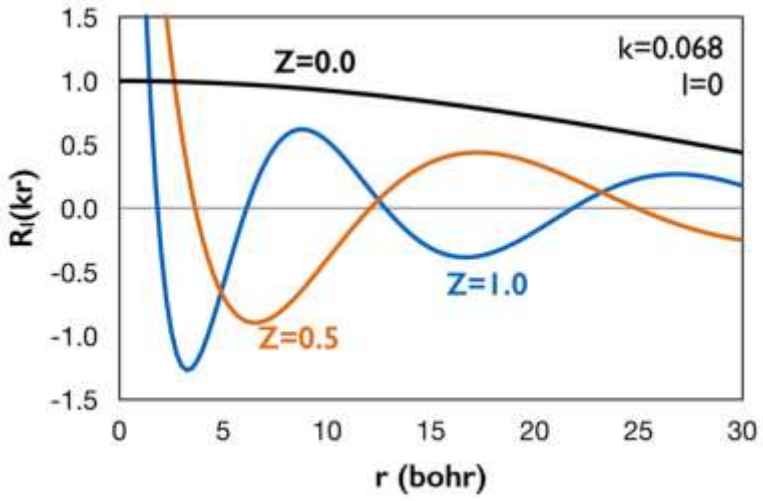

Figure 1.3.5 Coulomb radial function for l = 0 and k = 0.068 au (Ek = 0.0625 eV) with Z= 0.0 (black), 1.0 (blue), 0.5 (orange). The Coulomb radial function with Z = 0 is identical to the spherical bessel function of the plane wave. The Dyson orbitals of formaldehyde do not extend beyond 10 bohr.[34]

In summary, the study by Gozem *et al.* indicates that a single-center expansion of the photoelectron wave function and a PW or CW (often with an effective partial charge) can be used successfully to compute photoionization/photodetachment spectra with absolute total cross sections in reasonable agreement with experiments. However, the main problem is that the value of Z is difficult to predict without comparison with experiments. To develop predictive computational tools, it is desirable to have a method that can compute cross sections without any fitting parameters. Gozem *et al.* have discussed a potential algorithm to predict this partial charge. The purpose of this thesis work is to further explore this model and look for ways to develop it further.

Due to the limitations of existing methods for predicting the photoelectron spectra and the quest for more accurate *ab initio* methods in this field, we propose moving from a single center to a multi-center expansion of the photoelectron wave function. In the single-center

expansion discussed above, the photoelectron wave expansion is placed at the centroid of the Dyson orbital. For multi-center expansion, a photoelectron wave expansion is placed on each atom of the molecule. Following the example set by Gozem *et al.*, we also propose using Coulomb waves with partial charges, computed in a physically meaningful way, for each atom. The details of the methodology are provided in the following Theoretical and Computational Details section.

2 THEORETICAL AND COMPUTATIONAL DETAILS

2.1 Theoretical treatment of photoelectron spectroscopy:

Computing the probability of removing an electron from the system requires a theory for modeling the photoemitted electron. Often, the probability of ejecting an electron from the system is expressed as the total cross-section at a given energy. The photoelectron dipole matrix element connecting the initial and final states of the systems, introduced in equations (3)-(6), requires a Dyson orbital and wave function of the photoemitted electron to quantify the total cross-section of the system. Equation (6) can be expressed as a sum of its x,y,z components[39];

$$D_k^{IF} = \sum_{\alpha=x,y,z} \langle \phi^d | r_\alpha | \psi_k^{el} \rangle cos(\mu, e_\alpha), \ldots\ldots\ldots\ldots\ldots\ldots\ldots (7)$$

Here, r_α denotes the x, y, or z component of the dipole moment operator, and the cosine term represents the respective projections of the light polarization.

The Dyson orbital, which contains all the information about the initial and final states of the molecule, is an analog of a Hatree-Fock orbital describing the initial state of the ionized electron within Koopman's theorem.[27] Dyson orbitals can also be computed within the equation-of-motion coupled-cluster (EOM-CC) framework,[28] which provides accurate wave functions for closed-shell and various types of open-shell systems. EOM-CC Dyson orbitals included electron

correlation and orbital relaxation effects that are neglected in the Koopman's approximation.[26] The calculations in this thesis only address photoionization from a closed-shell system, which can usually be best described by the EOM-CC variant known as EOM-IP-CC (EOM-CC for ionization potentials).[27,28] The EOM-IP-CC is employed with single and double excitations, (EOM-IP-CCSD).

2.2 Computational simulation of photoelectron spectra:

So far, calculations and benchmarks using accurate (e.g., EOM-IP-CCSD) Dyson orbitals and approximate treatments of the photoelectron wave function have largely only used a single photoelectron wave function placed at the centroid of the Dyson orbital.[41] This is termed the "single center", or SC, approach. A multi-center (MC) approach has been proposed for the calculation of photoionization cross sections[42] and for the calculation of photoelectron angular[42,43] distributions.

In the present work, we will discuss both SC and MC approaches for modeling the photoelectron wave function in photoionization cross section calculations. These approaches will then be benchmarked for a series of small organic molecules for which experimental data is available.

The SC approach has been briefly discussed in the introduction section. A single plane or Coulomb wave (Figure 1.3.1) is used to describe the photoelectron wave function, depending on the charge and size of the molecule. However, to date, there is no clear predictive approach to estimate which effective charge should be used for molecules.

The center of expansion of the plane or Coulomb wave is often placed at the centroid of the Dyson orbital (e.g., see Figure 2.2.2). This is meant to ensure orthogonality.[31] However, in larger molecules, we may find in some instances that the center of expansion is not always

placed at a position where there is a high electron density (e.g., imagine a long alkene where the pi bond is mixed with many other sigma bonds along the alkane chain and the centroid of the Dyson orbital is far away from the double bond). A similar problem was discussed by Gozem *et al.* for delocalized water dimers or clusters,[43] where the center of expansion may be placed between water molecules rather than near the regions of high electron density.

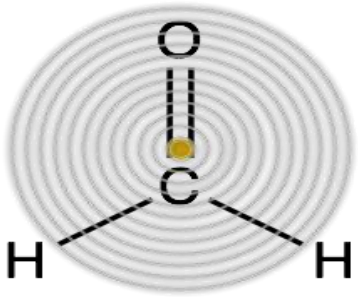

Figure 2.2.1 Example of a single-center expansion approach. The photoelectron wave expansion is centered on the centroid of the molecular Dyson orbital.

The MC approach is a natural solution to these problems mentioned above. In the MC approach, the Dyson orbital is fragmented into its atomic contributions. E.g., for a 4-atom molecule like formaldehyde, the Dyson orbital is divided into four orbitals, each completely localized on one of the atoms. Four photoelectron wave functions are then used, one at each atomic center, as shown in Figure 2.2.3. Each expansion only interacts with part of the Dyson orbital localized on that same atom. The advantage of the MC approach is that it ensures orthogonality of the photoelectron wave function to the orbitals of the atom it is centered on and avoids some of the problematic behaviors of the SC approach mentioned above.

The downside of using the MC approach is that it may be necessary to account for scattering (or coherences) between different atomic centers. It may also be necessary to account for overlap terms between the atomic centers. In this thesis, however, we will start with the

simplest MC model to probe how it performs compares to experimental PES of small organic molecules. In such a model, we will ignore scattering and overlap effects when computing the photoionization cross sections. This is justified if the overlaps terms are small (see discussion below) and assuming that scattering does not strongly affect the total cross section (only the angular distribution of the ejected electrons).

The photoelectron wave function can be treated as a Coulomb wave interacting with charge corresponding to the natural charge on the corresponding atom. Multiple ways exist to determine such an "effective charge" on each atom. In our work, we use natural charges obtained from a Natural Bond Analysis using a Natural Bond Orbital (NBO) calculation.[44] However, often the Dyson orbitals are delocalized on heavy atoms and not on the lighter hydrogen atoms. Therefore, we also tested another approach where we sum hydrogen charges onto the heavy atoms they are attached to. Hereon, this latter approach is referred to as the Heavy Atom Charge (HAC). We still use waves centered on the hydrogens but they interact with a 0 (zero) charge (typically the contribution of those waves to the total cross-section is very small because the magnitude of the Dyson on H atoms is small, so they have virtually no effect). Note that with the HAC approach, we also typically avoid having negative charges on atoms in almost all cases (whereas with NBO it is sometimes the case that heavy atoms have negative charges on them while the hydrogens are attached to them are positive). When we divide the molecular Dyson orbital into several parts, each localized on an atom, we are missing the overlaps between the different atom-centered orbitals, as indicated earlier. Therefore, the total norm of the orbital is reduced. In most cases, this reduction is small. For example, in formaldehyde, the total norm of the Dyson orbital as integrated is 1.000 (normalized). However, the sum of the squares of norms of the orbitals localized on each atom is 0.96, slightly reduced relative to the norm of the full

orbital. This missing norm is due to overlap terms. However, it is clear in this case that we capture most of the norm of the orbital using only the atomic terms with no overlaps.

In some cases, the sum of the squares of norms of the orbitals localized on each atom is significantly reduced. This is the case, for instance, in H_2, ethylene, and acetylene (typically where bonds are shared equally between atoms or groups). In those cases, the integrated norms are closer to ~0.7. In such cases, we may expect a larger error of the MC approach that doesn't account for overlap terms.

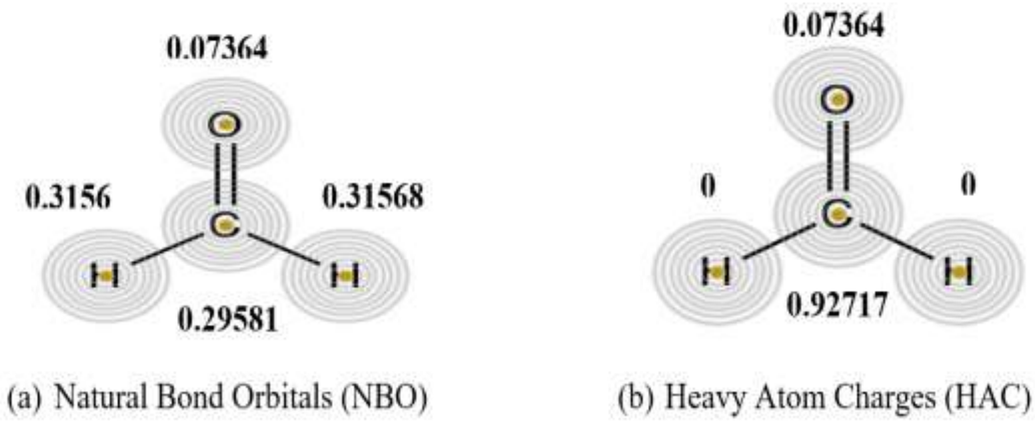

Figure 2.2.2 (a) NBO is the natural charge distribution of each atom. (b) HAC is derived from the NBO charges by summing the charges of the hydrogen atoms onto the heavy atom they are attached to.

When the center of expansion is placed on an atom with 0 charge (e.g., hydrogen atoms in the HAC approach), the photoelectron can simply be treated as the plane-wave (PW)[45];

$$\psi_k^{el} = \frac{1}{2\pi^{3/2}} e^{\mathrm{i}.\mathbf{kr}} \quad \ldots\ldots\ldots\ldots\ldots\ldots\ldots\ldots\ldots\ldots (8)$$

The $2\pi^{3/2}$ the factor is for continuum normalization, and is typically used for PWs. PWs can also be expressed as the sum of the spherical waves;

$$e^{i.kr} = 4\pi \sum_{l=0}^{\infty} \sum_{m=-1}^{l} i^l R_l(kr) Y_{lm}^*(\hat{r}) Y_{lm}(\hat{k}) \quad \ldots\ldots\ldots\ldots (9)$$

Here, $\hat{r}$ and $\hat{k}$ define the position vector and wave vector respectively. Each spherical wave is characterized by its energy $E = \frac{k^2}{2m}$, and angular momentum *l*, *m* and is a product of radial $R_l(kr)$ and spherical harmonic functions Y_{lm}. Radial functions can be expressed as spherical Bessel functions for plane waves, $R_l(kr) = j_l(kr)$. For the Coulomb wave, a Coulomb Radial function is used instead of spherical Bessel functions. The CW can also be expressed as the sum of Coulomb partial waves as in equation (9), except instead of using spherical Bessel functions, the radial part is described using a Coulomb radial wave function:[46]

$$R_l(kr,\eta) = (2kr)^l e^{-\pi\eta/2} \frac{|\Gamma(l+1+i\eta)|}{\Gamma(2l+2)} e^{-ikr} X\ {}_1F_1(l+1-i\eta, 2l+2, 2ikr) \quad \ldots\ldots\ldots\ldots\ldots\ldots\ldots\ldots (10)$$

where Γ is the Gamma function and ${}_1F_1$ is the confluent hypergeometric function of the first kind. η is the Sommerfeld parameter, which is equal to -Z/k in atomic units, where Z is the charge of the ionized core and k is the magnitude of the photoelectron wave vector. When Z = 0, the CW becomes a PW because the Coulomb radial function becomes equal to a spherical Bessel function.

In the MC approach, the origin of the PW or CW expansion is fixed at the nucleus of each atom, which ensures orthogonality with the electrons of that atom (i.e., Ψ^{el} is orthogonal to ϕ^d).

In this work, we have benchmarked several methods for computing near-threshold photoionization cross sections for small molecular systems that have reliable experimental cross-sections available. Specifically, we model the cross sections from the origin of the ionization up to a few electron volts above it. This region is sometimes considered as a key "fingerprint" region that is useful in identifying isomers in reactive mixtures.[47-49] We avoided systems that are likely to have autoionizing resonances near the threshold energy; the extension of EOM-CC theory to metastable electronic states can, in principle, be used to model these cases.[50]

Specifically, we test both the SC and MC approaches. SC results are reported both using a PW and CW with Z=1, with the center of expansion placed at the centroid of the Dyson orbital, following the protocol discussed by Gozem et al.[41] For the MC approach, we benchmarked both NBO and HAC approaches.

2.3 Inclusion of vibrational effects:

For all molecules studied in this work, density functional theory (DFT) is used to optimize the structures of the molecules with the ω-B97X-D functional[51]. The overlap between the ground and ionized states of molecular vibrations, largely responsible for the relative intensities of the vibrational bands in photoionization transitions, are called Franck-Condon-Factors (FCFs). The FCF is a vibrational overlap integral computed using geometries and vibrational frequencies of a molecule in the ground and ionized state. A change from one vibrational energy level to another one will be more likely to happen if the two vibrational wave functions overlap more significantly.[52] Classically, in terms of FCF approach, an electronic transition is most likely to occur without changes in the positions of the nuclei in the molecular entity and its environment. The resulting state is called a Franck–Condon state, and the transition involved, a vertical transition. The quantum mechanical formulation of this principle is that the intensity of a vibronic transition is proportional to the square of the overlap integral between the vibrational wavefunctions of the two states that are involved in the transition (Figure 2.3.1). Note that the vibration overlaps integral does not vanish by orthogonality because vibrational functions belong to different electronic states. In this thesis, we calculate FCFs using ezSpectrum.[53]

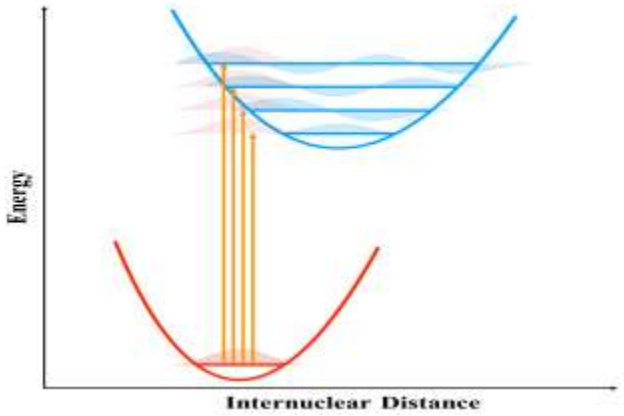

Figure 2.3.1 Franck-Condon factors associated with ionization (or any excitation). Vibrational excitations from the ground to excited molecular states are most intense when there is the largest overlap of ground and excited-state vibrational wave functions. Adapted from the figure by M.P Kabir, et al.[54]

2.4 Computational protocols:

This work will employ a mix of density functional theory (DFT) methods and EOM-CC methods for all calculations. The latter methods are particularly well-suited for computing excited states, ionized states, and radical/biradicals character associated with certain molecules.[55]

The EOM-CC method uses a single wave function to build on a robust size-consistent method by applying different operators to generate different types of final states.[30,56-58] More generally, EOM-CC is a many-body approach to account for the dynamical properties of atoms and molecules.[59] These dynamical properties include excitation energies and oscillator strengths in optical spectroscopy, the dynamic or frequency-dependent polarizability in light scattering studies, photoionization properties, and elastic and inelastic electron scattering properties.

Geometry optimizations of the ground (neutral) and ionized (positively charged radical) states were performed using the ω-B97X-D DFT method and aug-cc-pVTZ basis set. Q-Chem[29]

is used to generate Dyson orbitals, with the initial and final wave functions, Ψ_i^N and Ψ_F^{N-1}, described by CCSD and EOM-CCSD, respectively. The aug-cc-pVTZ basis set is used for the Dyson orbital calculations as well. Cross-sections are computed with ezDyson[32] using experimentally determined ionization energies. FCFs are computed by ezSpectrum[53] using DFT(ω-B97X-D)/aug-cc-pVTZ optimized structures and frequencies. The details about averaging over molecular orientations, accounting for electronic degeneracies of the initial and target states, and incorporating FCFs into the cross-section calculation can be found in ezDyson manual.[32]

3 RESULTS AND DISCUSSION

Two subsections are included in this results section. In the first section, we compare the simulated PES spectra (i.e., computed energy-dependent photoionization cross sections) for both the SC and MC treatments of photoelectron wave functions. In a second section, we compare the computed cross sections for a series of small alkenes and alkynes using the SC approach.

3.1 Single-center vs Multicenter treatment:

We have generated computational spectra with the SC (PW, CW with Z=1) and MC (NBO, HAC) approaches. The theory and backgrounds for those methods are discussed in Section 2. Shown in Figures 3.1.1 to 3.1.16 are the computed and experimental photoionization spectra for formaldehyde, 2,5-dihydrofuran, acetaldehyde, benzene, ethanol (vinyl alcohol), ethyl propionate, formic acid, furan, ketene, methanol, methyl acetate, methyl formate, and tetrahydrofuran, respectively.

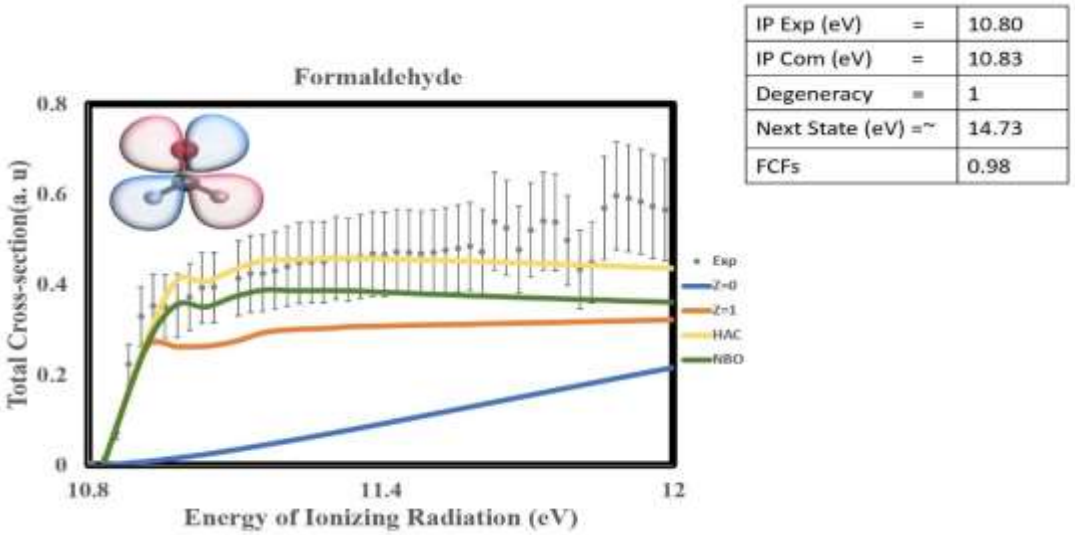

Figure 3.1.1 Computed (lines) and experimental[39] (dots) photoionization spectra of formaldehyde. Calculations are shown using a SC approach with PW (blue), Coulomb wave with Z=1 (orange), MC HAC (yellow), and MC NBO (green). The x-axis indicates the energy of ionizing radiation (eV), and the y-axis indicates the photoionization cross section (in atomic units). Photoionization cross sections are absolute and were not scaled.

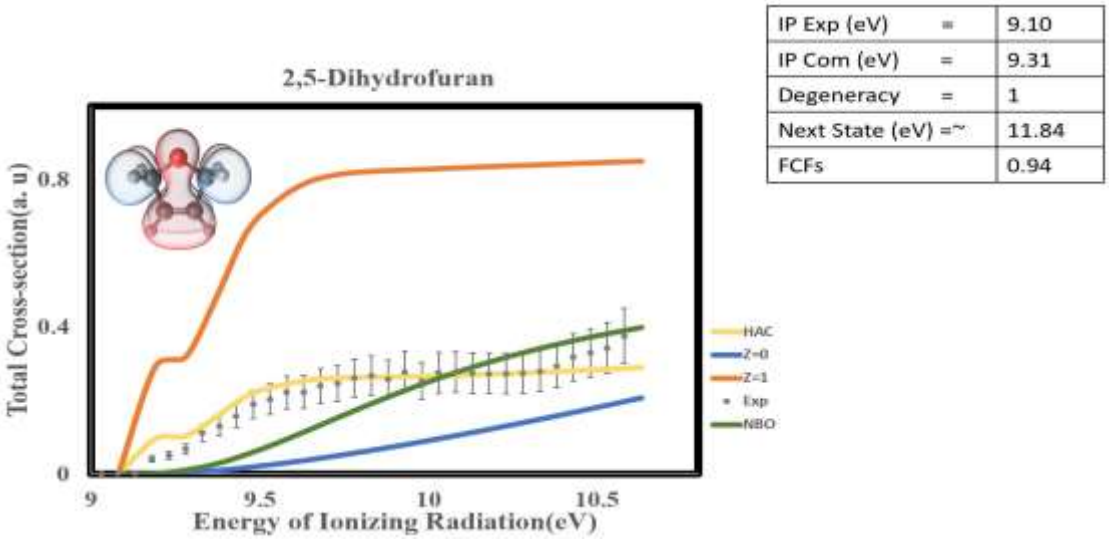

Figure 3.1.2 Computed (lines) and experimental[60] (dots) photoionization spectra of 2,5-Dihydrofuran. Calculations are shown using a SC approach with PW (blue), Coulomb wave with Z=1 (orange), MC HAC (yellow), and MC NBO (green).

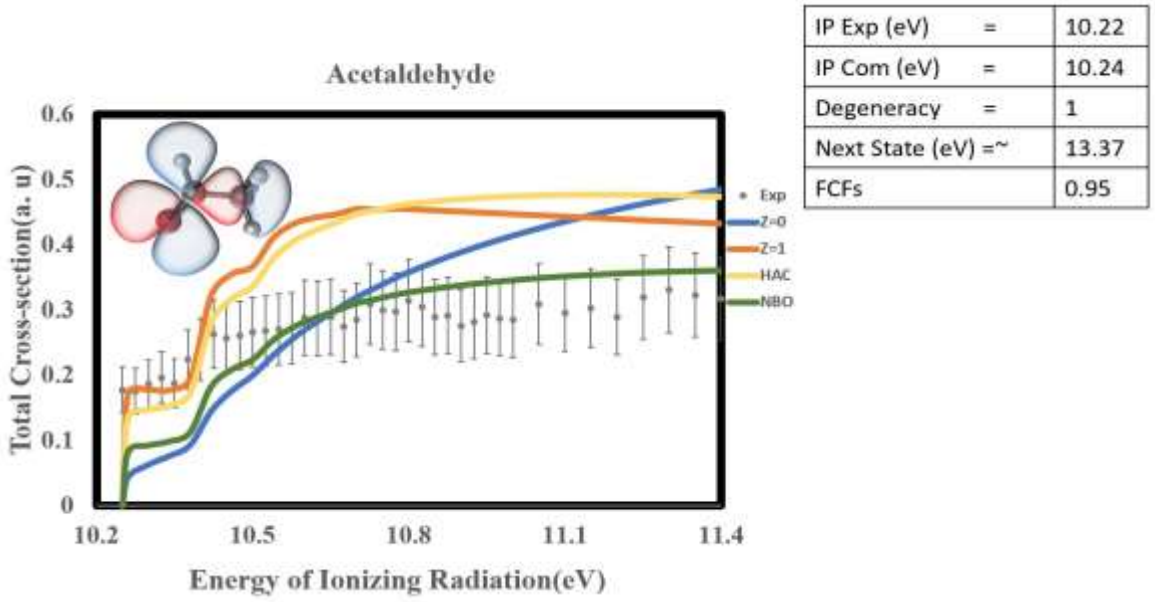

Figure 3.1.3 Computed (lines) and experimental[61] (dots) photoionization spectra of Acetaldehyde. Calculations are shown using a SC approach with PW (blue), Coulomb wave with Z=1 (orange), MC HAC (yellow), and MC NBO (green).

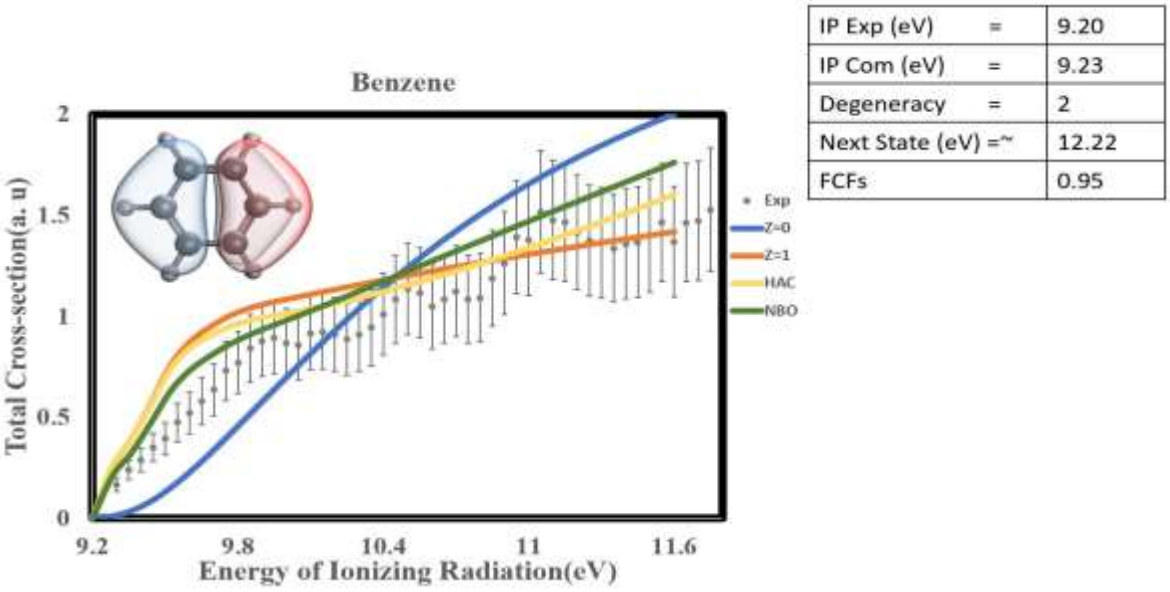

Figure 3.1.4 Computed (lines) and experimental[62] (dots) photoionization spectra of Benzene. Calculations are shown using a SC approach with PW (blue), Coulomb wave with Z=1 (orange), MC HAC (yellow), and MC NBO (green).

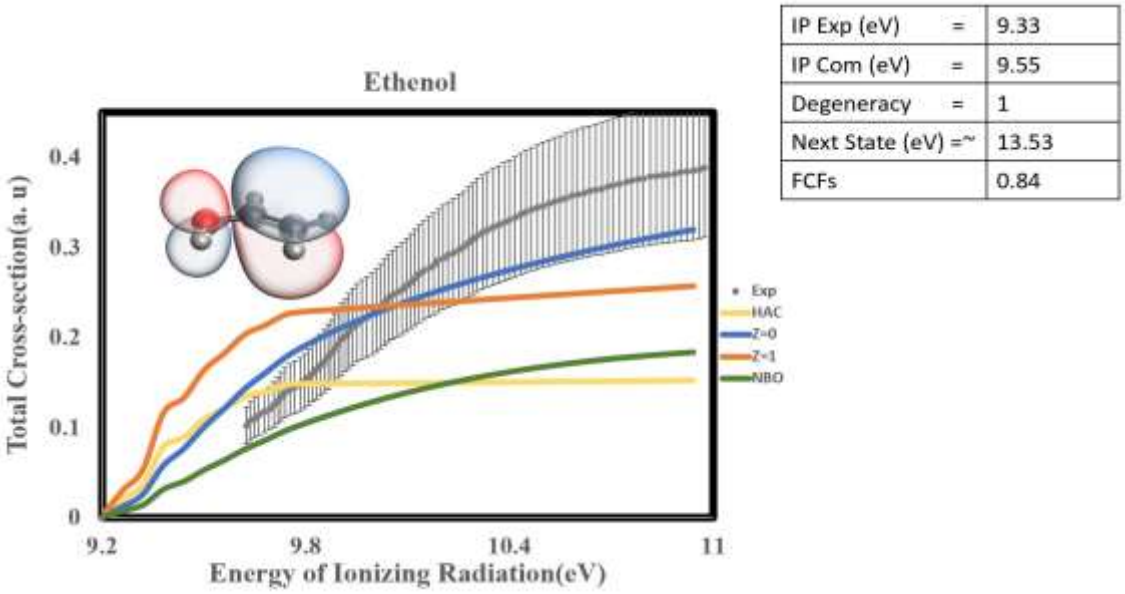

Figure 3.1.5 Computed (lines) and experimental[61] (dots) photoionization spectra of Ethenol. Calculations are shown using a SC approach with PW (blue), Coulomb wave with Z=1 (orange), MC HAC (yellow), and MC NBO (green).

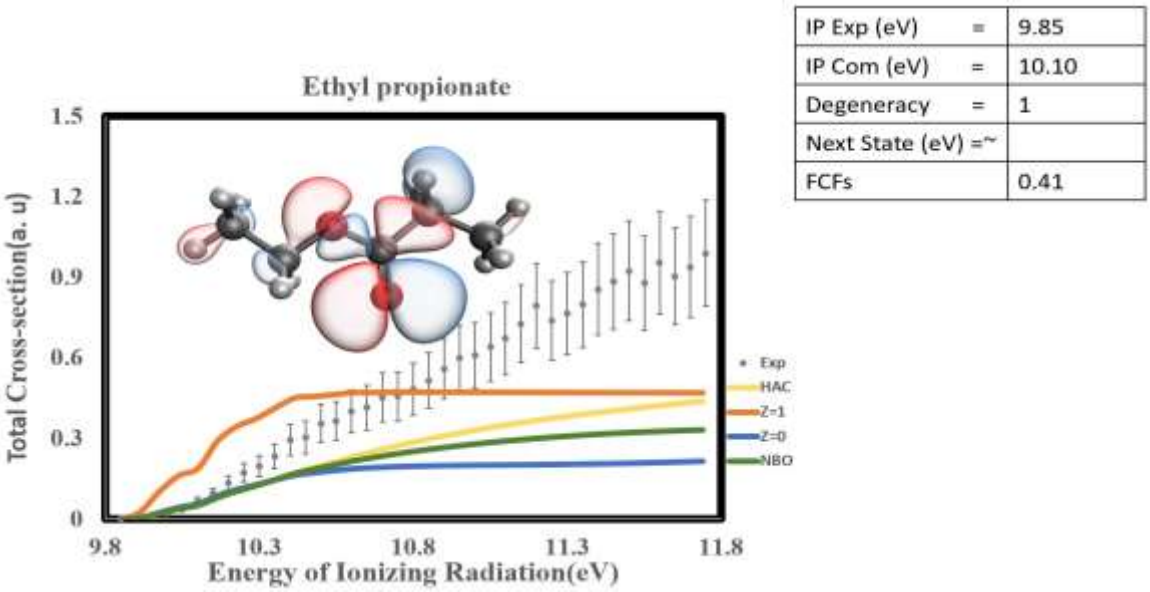

Figure 3.1.6 Computed (lines) and experimental[63] (dots) photoionization spectra of Ethyl propionate. Calculations are shown using a SC approach with PW (blue), Coulomb wave with Z=1 (orange), MC HAC (yellow), and MC NBO (green).

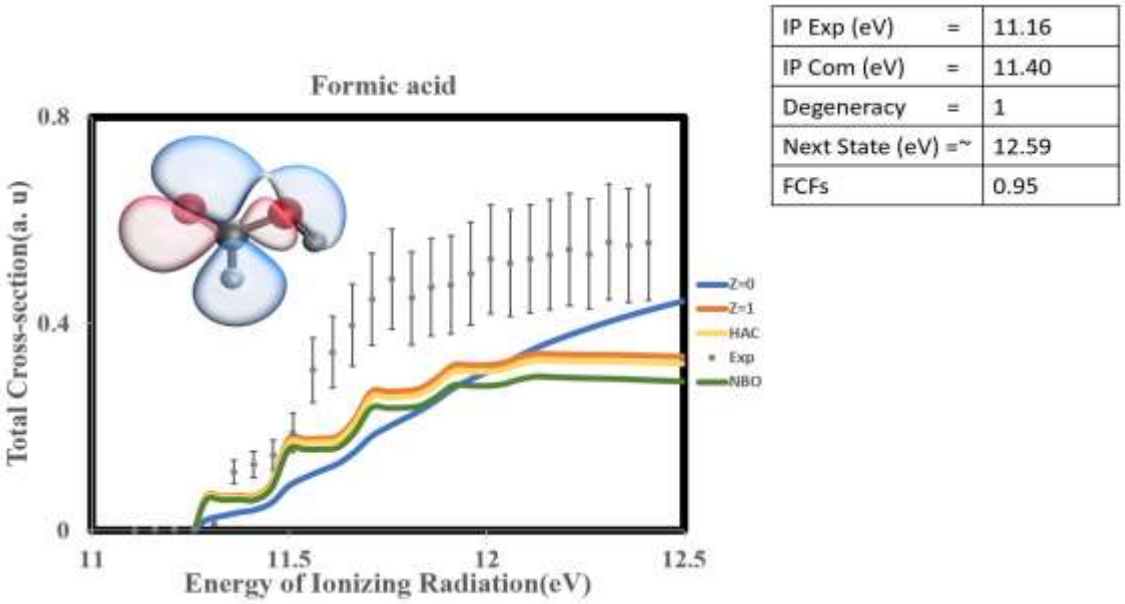

Figure 3.1.7 Computed (lines) and experimental[63] (dots) photoionization spectra of Formic acid. Calculations are shown using a SC approach with PW (blue), Coulomb wave with Z=1 (orange), MC HAC (yellow), and MC NBO (green)

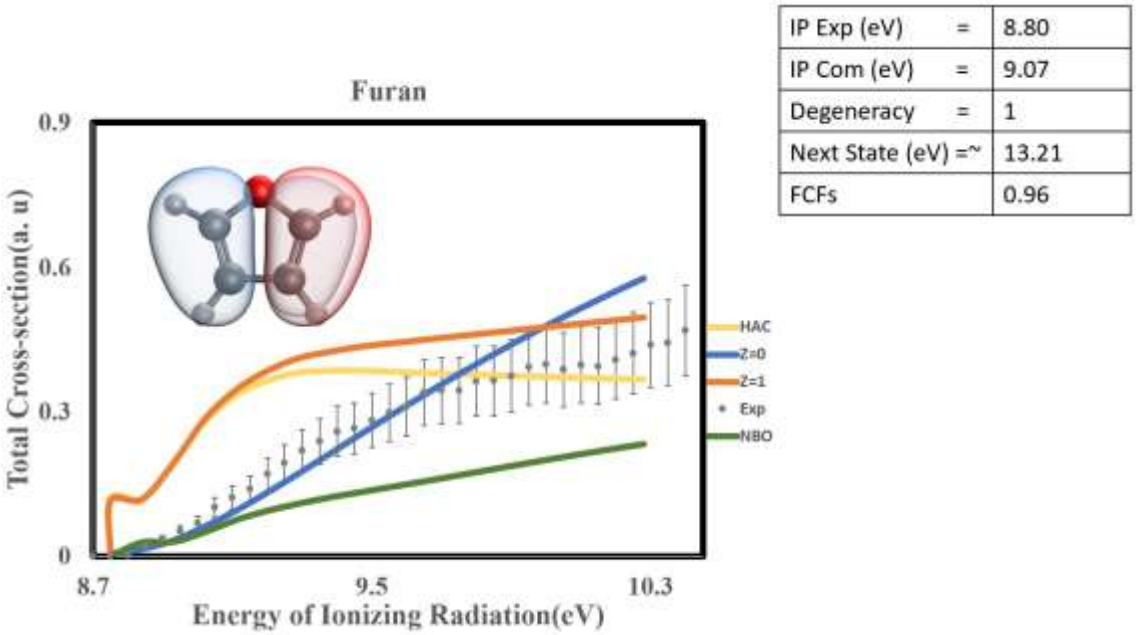

Figure 3.1.8 Computed (lines) and experimental[60] (dots) photoionization spectra of Furan. Calculations are shown using a SC approach with PW (blue), Coulomb wave with Z=1 (orange), MC HAC (yellow), and MC NBO (green).

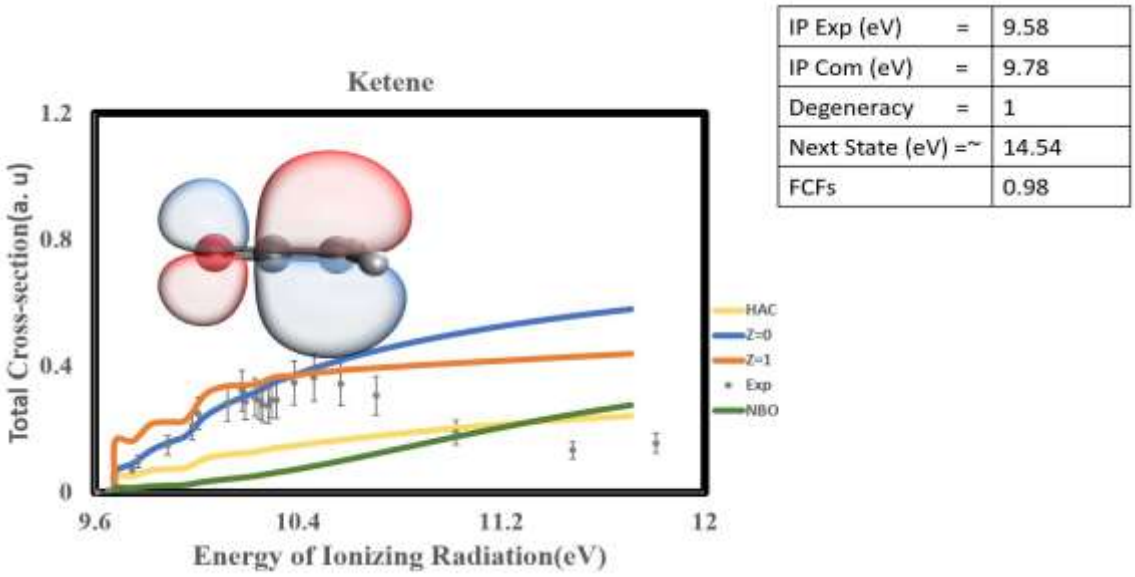

Figure 3.1.9 Computed (lines) and experimental[60] (dots) photoionization spectra of Ketene. Calculations are shown using a SC approach with PW (blue), Coulomb wave with Z=1 (orange), MC HAC (yellow), and MC NBO (green).

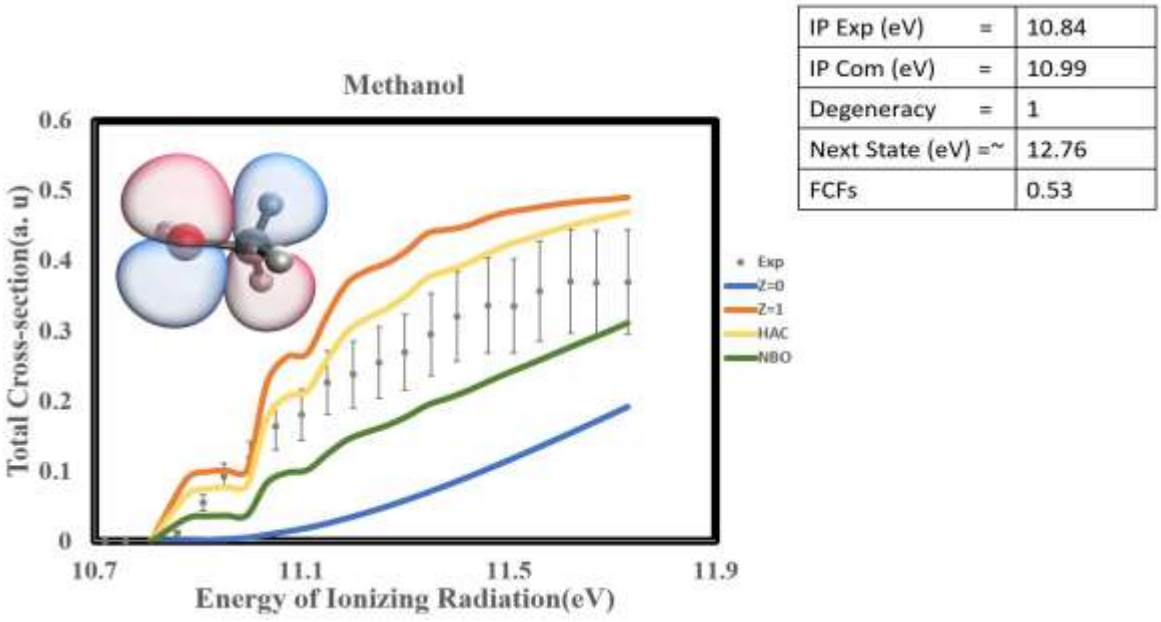

Figure 3.1.10 Computed (lines) and experimental[62] (dots) photoionization spectra of Methanol. Calculations are shown using a SC approach with PW (blue), Coulomb wave with Z=1 (orange), MC HAC (yellow), and MC NBO (green).

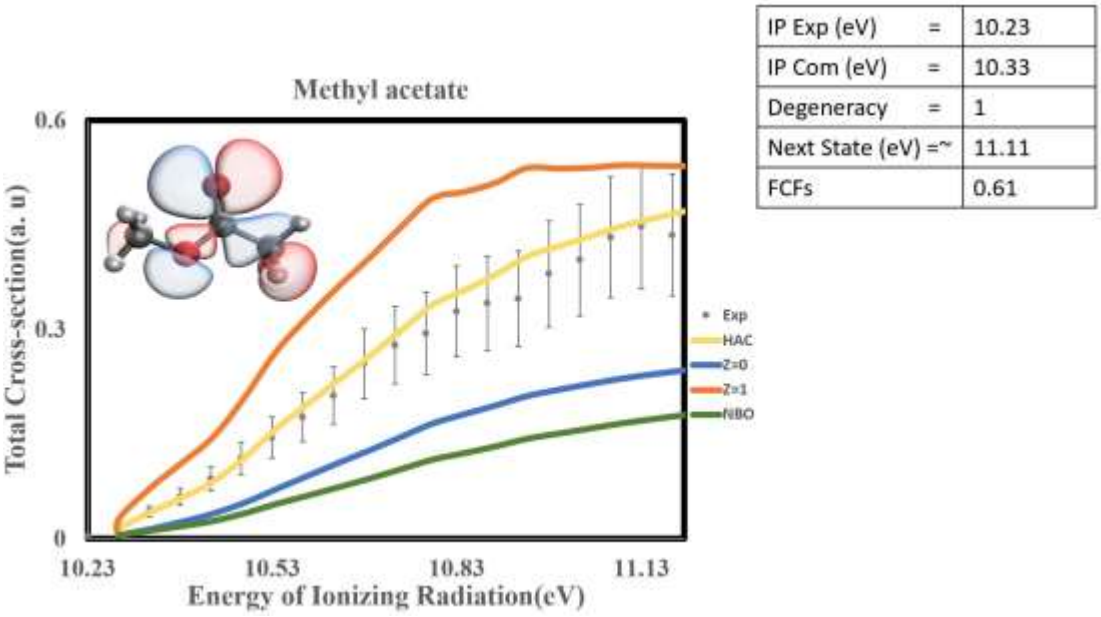

Figure 3.1.11 Computed (lines) and experimental[64] (dots) photoionization spectra of Methyl acetate. Calculations are shown using a SC approach with PW (blue), Coulomb wave with Z=1 (orange), MC HAC (yellow), and MC NBO (green).

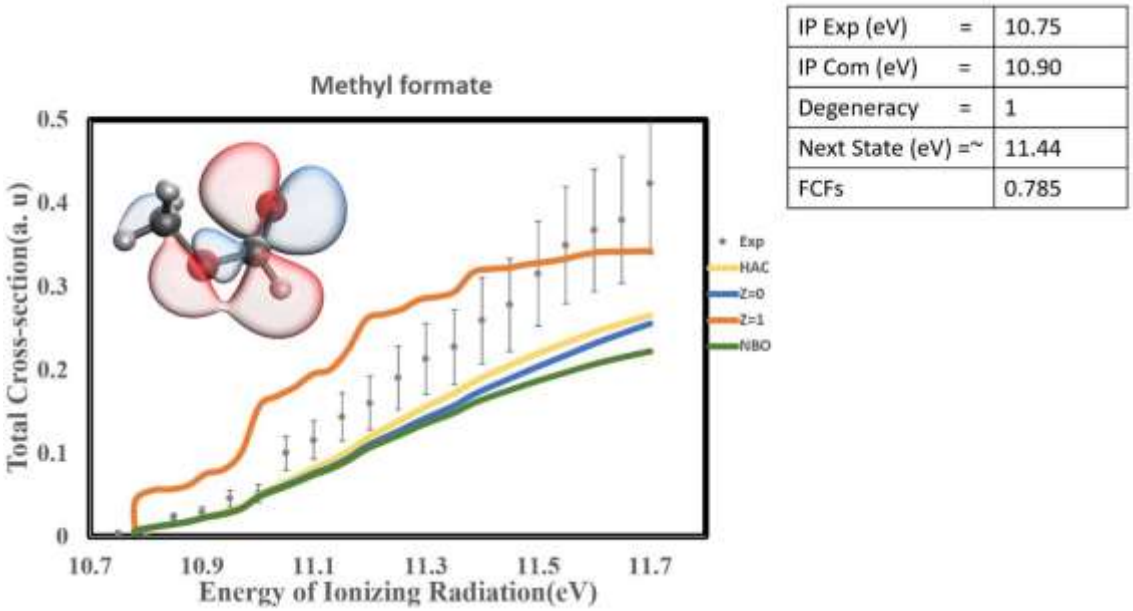

Figure 3.1.12 Computed (lines) and experimental[63] (dots) photoionization spectra of Methyl formate. Calculations are shown using a SC approach with PW (blue), Coulomb wave with Z=1 (orange), MC HAC (yellow), and MC NBO (green).

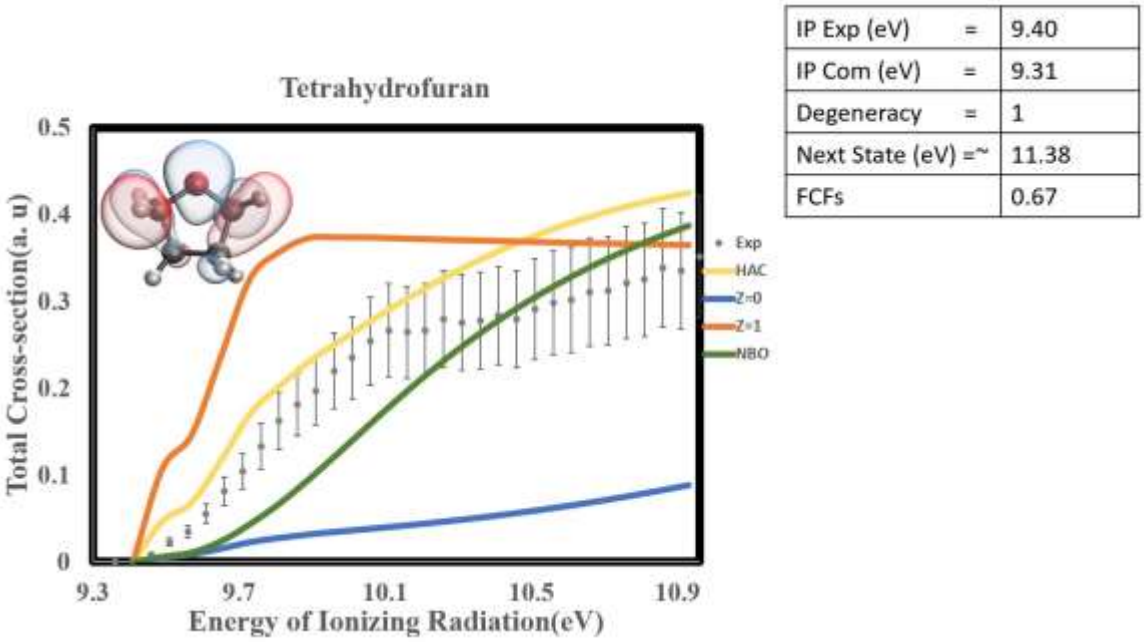

Figure 3.1.13 Computed (lines) and experimental[64] (dots) photoionization spectra of Tetrahydrofuran. Calculations are shown using a SC approach with PW (blue), Coulomb wave with Z=1 (orange), MC HAC (yellow), and MC NBO (green).

In multiple cases, NBO and HAC outperform the SC approaches, giving a better result than Z=0 and Z=1. Often, HAC also outperforms the NBO approach, and in some cases provides cross sections that are in quantitative agreement with the experiments (within the experimental error). There are a few notable exceptions, however, including ethyl propionate, furan, and ketene. Overall, however, the HAC approach does not provide highly unreasonable artifacts or unrealistic cross sections, indicating that it is a reasonable approach for further pursuit, refinement, and benchmarking.

There are multiple sources of error that complicate the comparison between computations and experiments. Those are:

a) **Missing overlap terms**. In the computational approach used here, a simple MC approach is used where the overlap terms between orbitals centered on different atoms are neglected. Accounting for the overlap terms may improve the results of the calculations.

b) **Other deficiencies of the computational model**. The photoionization cross section is still computed using an approximate photoelectron wave function employing a Coulomb wave with an effective charge derived from natural charge calculations.

c) **Experimental resonant autoionizing states**. The calculations only account for direct photoionization cross sections. However, experimental spectra include both direct photoioniozation as well as autoionization from resonance (metastable) states. Such states may increase the photoionization cross section if they exist near the ionization threshold. One example of where this occurs is ketene, where the bump at around 11.45 eV may be attributed to a resonance state. Other molecules may have other similar but more broadened low-lying autoionizing states.

d) **Experimental errors**. The measurement of photoionization cross sections is not straightforward and requires accurate measurements of the pressure of the system. Often, experiments have a relatively large (e.g., 20%) error, as indicated by the error bars in Figures 3.1.1 – 3.1.6. [62] Sometimes different experiments are not full internally consistent. This makes it difficult to quantify the exact error from calculations relative to experiments.

For the reasons above, it is not easy to quantify the error of computations relative to experiments without doing more extensive benchmarks against more molecules and using more computational methods to check for consistency.

3.2 Comparison of Cross sections of alkenes and alkynes:

Alkenes and Alkynes has almost identical Dyson orbitals. In Figure 3.2.1, we show a plot of a r x the Dyson orbital for the ethylene and acetylene along an axis going through the center of the C-C bond. Acetylene has just a little more electron density near the middle of the bond, but the difference does not appear large enough to justify very different cross sections. Therefore, it would be expected that ethylene and acetylene would have a similar cross section for ionization of a single pi orbital.

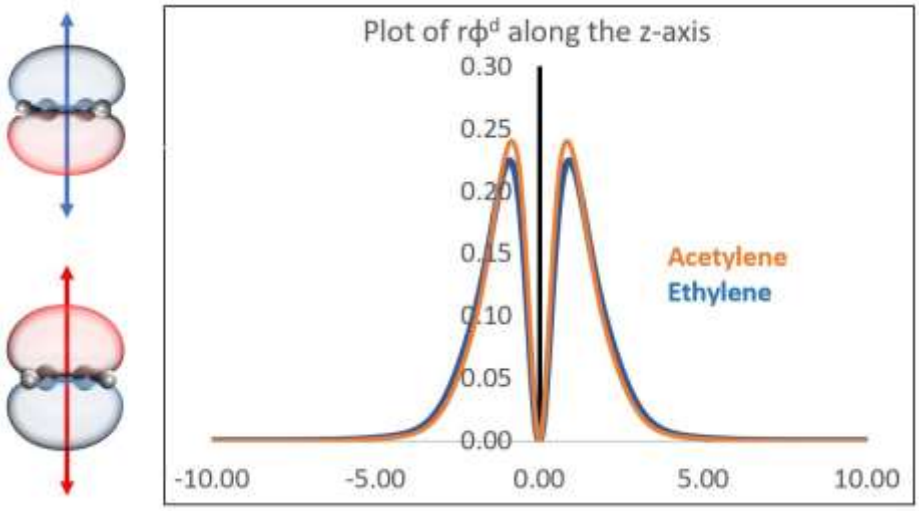

Figure 3.2.1 Plot of Dyson orbitals of ethylene and acetylene along the axis indicated using arrows on the figures on the left.

Note, however, that acetylene has two degenerate pi orbitals while ethylene has only one pi orbital. Therefore, statistically, acetylene is twice as likely to be ionized relative to ethylene. We can therefore expect that the cross sections of acetylene (and related alkynes) will be approximately double that of ethylene (and related alkenes). While this is observed computationally in our models, in many alkenes and alkynes this is not observed experimentally, as shown in Figures 3.2.2 – 3.2.5.

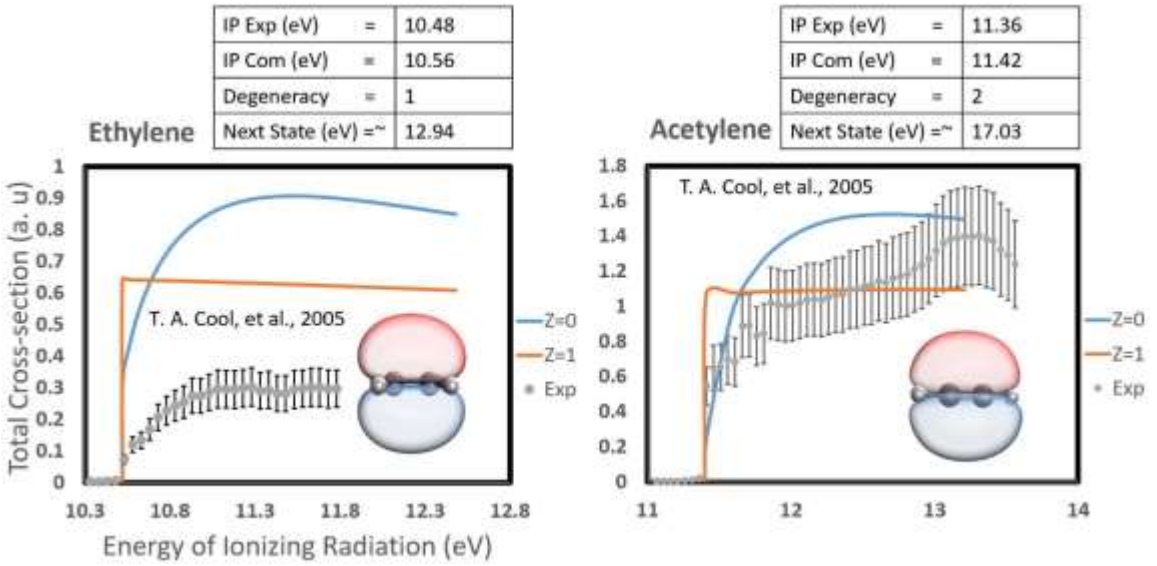

Figure 3.2.2 Comparison of the computed (lines) and experimental[62] (dots) photoionization spectra of acetylene and ethylene. Calculations are only shown for SC approach with PW (blue), Coulomb wave with Z=1 (orange). Note that FCFs are not included here.

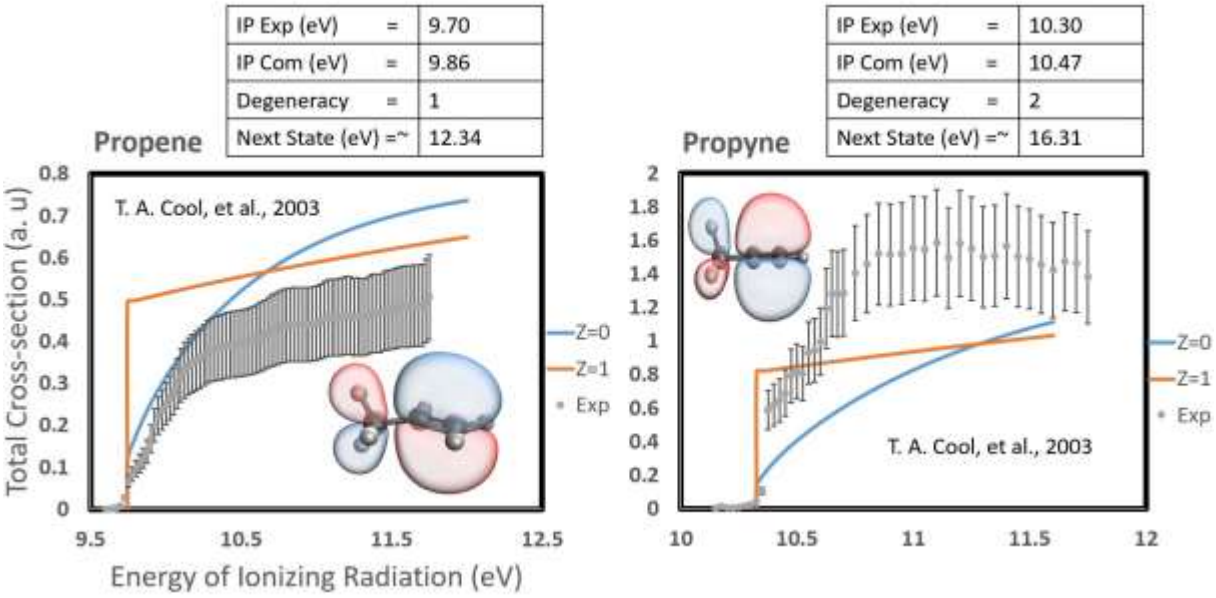

Figure 3.2.3 Comparison of the computed (lines) and experimental[61] (dots) photoionization spectra of propene and propyne. Calculations are only shown for SC approach with PW (blue), Coulomb wave with Z=1 (orange). Note that FCFs are not included here.

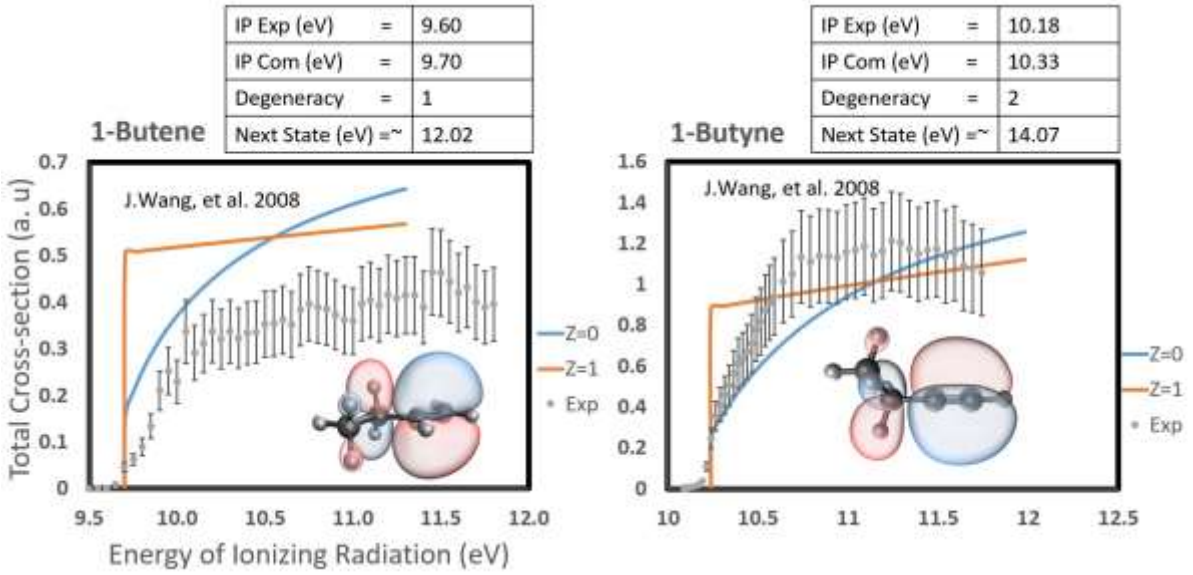

Figure 3.2.4 Comparison of the computed (lines) and experimental[64] (dots) photoionization spectra of 1-butene and 1-butyne. Calculations are only shown for SC approach with PW (blue), Coulomb wave with Z=1 (orange). Note that FCFs are not included here.

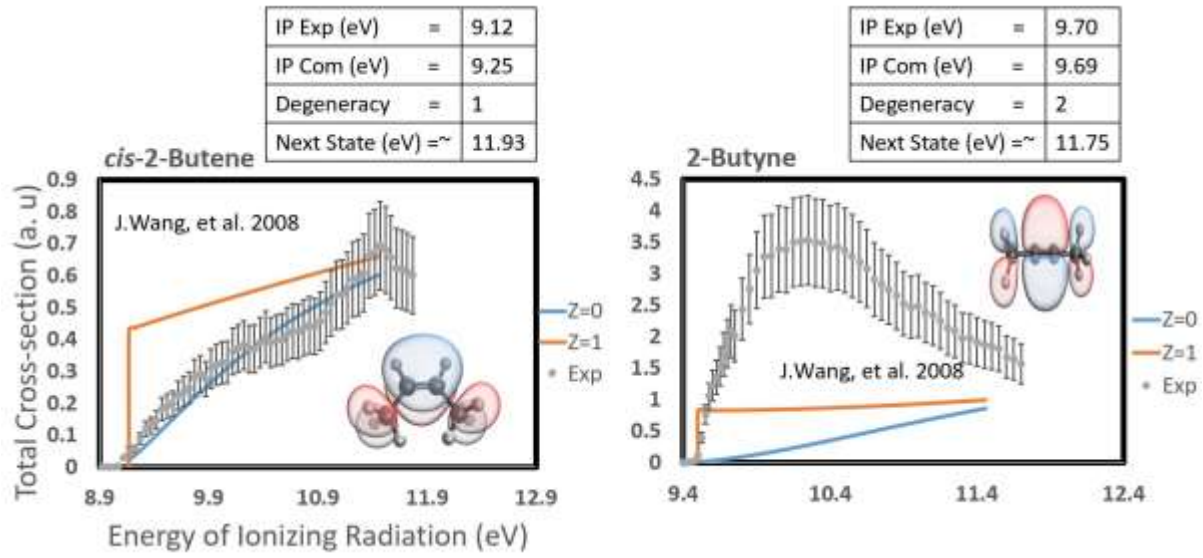

Figure 3.2.5 Comparison of the computed (lines) and experimental[64] (dots) photoionization spectra of *cis*-2-butene and 2-butyne. Calculations are only shown for SC approach with PW (blue), Coulomb wave with Z=1 (orange). Note that FCFs are not included here.

In Figures 3.2.2 – 3.2.5, only a SC PW or CW approach is used. We note that the absolute cross sections computed for alkynes are approximately two times larger than the absolute cross sections computed in alkenes, as anticipated earlier. However, when we compare experimental and computed cross sections, we note that calculations on alkenes overestimate the photoionization cross sections relative to the experiment, while computations for alkynes underestimate the cross sections relative to experiments. This indicates that experimental cross sections are not related by simply a factor of 2 when comparing alkenes and alkynes. In fact, sometimes alkynes have an at least 3-4 times larger cross section than alkenes. While this may point a problem with an oversimplified computational model, a more likely (and, to some extent, experimentally supported) explanation is that alkynes have low-lying metastable states that do not exist in alkenes. Indeed, low-lying metastable states have been discussed in multiple alkynes.[65]

4 CONCLUSIONS

Total photoionization cross sections for the small organic neutral molecules have been calculated with a single center approach (using both plane and Coulomb waves) and a multi-center approach (using natural charges derived from Natural bond analysis, both with and without hydrogen charges summed onto heavy atoms). The calculation of the total cross-sections by a multi-center approach often yields a better agreement with experimental photoionization spectra compared to single-center approaches, but it is not consistent for all the molecules. While comparing cross sections of alkenes and alkynes, however we saw alkynes have experimental cross sections that are often 3-4 times larger than those of alkenes. Theoretically, we expect that alkyne cross sections should only be twice larger than those of

alkanes. This implicates possible low-lying resonance states near the threshold ionization region in alkynes. There is some experimental evidence to support this conclusion.[65]

To build on the work in this thesis, several approaches are possible. First, it is desirable to test the effect of including overlap terms in the calculations of photoionization cross sections. Second, more extensive benchmarking is needed to determine the most appropriate computational approach. Third, experimental data must be carefully examined to rule out involvement of resonance states or experimental errors. If resonance states cannot be ruled out experimentally, the extension of EOM-CC theory to metastable electronic states can be used to model these cases.[50]

REFERENCES

1. Turner DW. Molecular Photoelctron Spectroscopy. *Philosophical Transactions of the Royal Society of London.* 1970;268, No- 1184:7-31.
2. Berkowitz J. *Photoabsorption, Photoionization and Photoelctron Spectroscopy.* 1st ed. 111, fifth Avenue, New York, New York , 10003: Academic Press; 1979.
3. Stefan Ha. *Photoelectron spectroscopy: Principles and application.* Springer; 2003.
4. Compendium of Chemical Terminology : "Photoelectron Spectroscopy". 1997. Published 2nd.
5. Raczyński A, Zaremba J. Threshold effects in Photoionization and Photodetachment. *Physics Report.* 1993;235(1):1-55.
6. BEYNON JDE. An Experimental Determination of the Photo-ionization Cross-section of Atomic Hydrogen. *Nature.* 1965;207.
7. Libretext Librarys. https://chem.libretexts.org/Courses/Pacific_Union_College/Quantum_Chemistry/10%3A_Bonding_in_Polyatomic_Molecules/10.04%3A_Photoelectron_Spectroscopy. Accessed.
8. Peter Atkins JdP. *Physical Chemistry (Thermodynamics, Structure and Changes).* 10th ed: W.H. Freeman and Company; 2014.
9. G.Greczynski LH. X-ray photoelectron spectroscopy: Towards reliable binding energy referencing. *Elsevier.* 2019;107:100591.
10. Randy L. Vander Wal VMB, and Michael D. Hays. XPS Analysis of Combustion Aerosols for Chemical Composition, Surface Chemistry, and Carbon Chemical State. *Analytical Chemistry.* 2011;83,6:1924-1930.
11. Jason K Cooper CDG, Jin Z Zhang. Ab initio calculation of ionization potential and electron affinity of six common explosive compounds. *Theoretical Chemistry.* 2012;1:11-19.
12. F Buonocore FT, D Ninno, A Di Matteo, G Cantele and G Iadonisi Ab initio calculations of electron affinity and ionization potential of carbon nanotubes. *Nanotechnology.* 2007;19, number 2.
13. Albert Stolow AEB, and Daniel M. Neumark. Femtosecond Time-Resolved Photoelectron Spectroscopy. *Chemical review.* 2004;104,4:1719-1758.
14. Richard Mabbs ERG, Kostyantyn Pichugin, Andrei Sanov. Photoelectron imaging: an experimental window into electronic structure. *Chemical Society Reviews.* 2009;38(8):2169-2177.
15. Jobory Ta. NMR-Relaxation Mechanisms of O17 in Aqueous Solutions of Paramagnetic Cations and the Lifetime of Water Molecules in the First Coordination Sphere *Journal of Chemical Physics.* 1962;45:4256.
16. Eland JHD. *Photoelectron spectroscopy.* second ed. Great Britain, Southempton: Butterworth and Co (publishers) Ltd; 1984.
17. L.J.Gerenser RCB. Study of chemisorption on silver surfaces using ultraviolet photoelectron spectroscopy (UPS). *Elsevier.* 1980;2(2):259-268.
18. J.F.Moulder WFS, P.E.Sobol, and K.D.Bomben. *Handbook of X-ray Photoelectron Spectroscopy.* Eden Prairie, MN, USA: Perkin Elmer Corp.; 1992.
19. D.N. Nanda KJ. SINDO1. A semiempirical SCF MO method for molecular binding energy and geometry I. Approximations and parametrization. *Springer Link.* 1980;57:95-106.

20. Suwipa Saen-oon MK, Supa Hannongbua. Binding energy analysis for wild-type and Y181C mutant HIV-1 RT/8-Cl TIBO complex structures: Quantum chemical calculations based on the ONIOM method *Willey Online Library.* 2005.
21. Ruberti MA, V.; Decleva, P. B-spline algebraicdiagrammatic construction: Application to photoionization crosssections and high-order harmonic generation. *Journal of Chemical Physics.* 2014;141:164126.
22. Langhoff PWR, T., McKoy, V., Schneider, B., Eds. *In Electron Molecule and Photon Molecule Collisions.* Plenum Press: New York1979.
23. Cacelli IM, R.; Rizzo,. Gaussian-type-orbital basis sets for the calculation of continuum properties in molecules: The differential photoionization cross section of molecular nitrogen. *Physical Review A : At, Mol, Opt Phys.* 1998;57:1895-1905.
24. Ortiz JV. Toward an exact one-electron picture of chemical bonding. *Advance Quantum Chem.* 1999;33:33-52.
25. Ortiz JV. *Computational Chemistry: Reviews of Current Trends.* World Scientific Publishing Co Pte Ltd; 1997.
26. Krylov AI. Equation-of-motion coupled-cluster methods for open-shell and electronically excited species: The hitchhiker's guide to Fock space. *Annu Rev Phys Chem.* 2008;59:433−462.
27. Sneskov KC, O. Excited state coupled cluster methods. *WIREs CompMol Sci.* 2012;2:566.
28. Bartlett RJ. Coupled-cluster theory and its equation-of-motion extensions. *WIREs CompMol Sci.* 2012;2:126-138.
29. Shao YG, Z.; Epifanovsky, E.; Gilbert, A. T. B.; Wormit, M.; Kussmann, J.; Lange, A. W.; Behn, A.; Deng, J.; Feng, X.; et al. Advances in molecular quantum chemistry contained in the Q-Chem 4 program package. *Mol Phys.* 2015;113:184−215.
30. Gozem SM, F.; Lindh, R.; Krylov, A. I.; Granovsky, A. A.; Angeli, C.; Olivucci. *M, J Chem Theory Comput.* 2013;9(10):4495-4506.
31. C. Melania Oanna AIK. Dyson orbitals for ionization from the ground and electronically excited states within equation-of-motion coupled-cluster formalism: Theory, implementation, and examples *Journal of Chemical Physics.* 2007;127:234106.
32. Gozem SK, A. I. ezDyson Manual. In:2015.
33. A. V. Arecchi TM, and R. J. Koshel. *Field Guide to Illumination.* Bellingham, WA: SPIE press; 2007.
34. Samer Gozem AOG, , Takatoshi ichino, David L. Osborn, John F stanton. Photoelctron wave function in photoionization: plane wave or coulomb wave. *THe journal of Physical Chemistry letter.* 2015;6,22:4532-4540.
35. H.G.M.Heideman MLHH, C.Smit. Resonance excitation of helium by electrons at energies near 60 eV. *Physica.* 1970;47(1):159-164.
36. Samson JAR. Photoionization of atoms and molecules. *Methods Exp Phys.* 1976;13:204.
37. J.A.R. Samson WCS. Precision measurements of the total photoionization cross-sections of He, Ne, Ar, Kr, and Xe. *Journal of electron spectroscopy and related phenomenon.* 2002;123(2-3):265-276.
38. Smith LMBaSJ. Experimental Cross Section for Photodetachment of Electrons from H− and D−. *Phys Rev.* 1955;98:1028.

39. Dodson LGS, L.; Savee, J. D.; Eddingsaas, N. C.; Welz, O.; Taatjes, C. A.; Osborn, D. L.; Sander, S. P.; Okumura, M.V. UV photoionization cross sections of HO2, H2O2, and H2CO. *Journal of Physical Chem A.* 2015;119:1279-1291.
40. . 2018 CODATA Value: Bohr radius". The NIST Reference on Constants, Units, and Uncertainty. NIST. 20 May 2019. Retrieved 2019-05-20.
41. Samer Gozem FM, Alessio Valentini, Michael Filatov, Miquel Huix-Rotllant, Nicolas Ferré, Luis Manuel Frutos, Celestino Angeli, Anna I Krylov, Alexander A Granovsky, Roland Lindh, Massimo Olivucci. Shape of multireference, equation-of-motion coupled-cluster, and density functional theory potential energy surfaces at a conical intersection. *Journal of chemical theory and computation.* 2014;10(8):3074-3084.
42. Lara Martini DIRBaOAF. Interferences in the photoionization of water molecules. *Journal of Chemical Physics B: Atomic, Molecular and Optical Physics.* 2019;52(10).
43. Samer Gozem RS, Uwe Hergenhahn, Evgeny Lugovoy, Bernd Abel, Bernd Winter, Anna I Krylov, Stephen E Bradforth. Probing the Electronic Structure of Bulk Water at the Molecular Lengthscale with Angle-Resolved Photoelectron Spectroscopy. *THe journal of Physical Chemistry letter.* 2020;11(13):5162-5170.
44. Natural bond orbital methods. Wiley Online library; 2011. https://onlinelibrary.wiley.com/doi/abs/10.1002/wcms.51.
45. Gingrich DM. Practical Quantum Electrodynamics;. *CRC Press: Boca Raton, FL.* 2006.
46. Landau LD, Liftshiz, E. M. *Quantum Mechanics: Non-relativistic theory;.* Pergamon: Oxford.
47. Bodi AH, P.; Osborn, D. L.; Sztaray, B. Massresolved isomer-selective chemical analysis with imaging photoelectronphotoion coincidence spectroscopy. *J Phys Chem Lett.* 2013;4:2948−2952.
48. Lockyear JFW, O.; Savee, J. D.; Goulay, F.; Trevitt, A. J.;, Taatjes CAO, D. L.; Leone, S. R. Isomer specific product detection in the reaction of CH with acrolein. *J Phys Chem A.* 2013;117:11013−11026.
49. Welz OZ, J.; Savee, J. D.; Sheps, L.; Osborn, D. L.; Taatjes, C. A. . .Low-temperature combustion chemistry of n-butanol:Principal oxidation pathways of hydroxybutyl radicals. *J Phys Chem A.* 2013;5:11983−12001.
50. Jagau T-CZ, D.; Bravaya, K. B.; Epifanovsky, E.; Krylov,, I. A. A fresh look at resonances and complex absorbing potentials:Density matrix based approach. *J Phys Chem Lett.* 2014;5:310-315.
51. Chai J-DH-G, M. Long-range corrected hybrid density functionals with damped atom-atom dispersion interactions. *Phys Chem Chem Phys.* 2008(10):6615−6620.
52. Franck J. Elementary processes of photochemical reactions. In. Vol 21: Transactions of the Faraday Society; 1926:536-542.
53. Mozhayskiy VAK, A. I. ezSpectrum. In:2015.
54. Kabir MPO-G, Y.; Gozem, S. Spectra of Flavin in Different Redox and Protonation States: A Computational Perspective on the Effect of the Electrostatic Environment. *Phys Chem Chem Phys.* 2019;21(30):16526-16537.
55. Rebeca N Johnson SG. *Photoelectron spectra and formation Mechanism of interstellar C3H20 isomers from Quantum mechanical calculations*. Scholarwork@Georgia State University: Chemistry, Georgia State University; 2019.
56. Krylov AI. *Annu Rev Phys Chem.* 2008;59:433-462.
57. Krylov AI. *Acc Chem Res.* 2006;39(2):83-91.

58. Gozem SK, A. I.; Olivucci. *M, J Chem Theory Comput.* 2012;9(1):284-292.
59. McCurdy C.W. RTN, Yeager D.L., McKoy V. *The Equations of Motion Method: An Approach to the Dynamical Properties of Atoms and Molecules.* Vol 3. Boston, MA: Springer; 1977.
60. Bin Yang JW, Terrill A.Cool, Nils Hansen, Scott Skeen, David L.Osborn. Absolute photoionization cross-sections of some combustion intermediates. *Int J Mass Spectrum.* 2012;309:118-128.
61. Terrill A. Cool KN, and Toufik A. Mostefaoui Selective detection of isomers with photoionization mass spectrometry for studies of hydrocarbon flame chemistry *Journal of Chemical Physics.* 2003;119(16):8356-8365.
62. Cool TA, ; Wang, J.; Nakajima, K.; Taatjes, C.A.; Mcllory, A. Photoionization cross-section for reaction intermediates in hydrocarbon combustion. *Int J Mass Spectrum.* 2005;247:18-27.
63. Juan Wang BY, Terrill A.Cool, Nils Hansen. Absolute cross-sections for dissociative photoionization of some small esters. *Int J Mass Spectrum.* 2010;292(1-3):14-22.
64. Wang JY, B.; Cool, T. A.; Hansen, N.; Kasper, T. Near-Threshold Absolute Photoionization Cross-Sections of Some Reaction Intermediates in Combustion. *Int J Mass Spectrum.* 2008;269(3):210-220.
65. U. Jacovella DMPH, S. Boyé-Péronne, Bérenger Gans, N. de Oliveira, K. Ito, D. Joyeux, L. E. Archer, R. R. Lucchese, Hong Xu, and S. T. Pratt. A Near-Threshold Shape Resonance in the Valence-Shell Photoabsorption of Linear Alkynes. *J Phys Chem A.* 2015;119(50):12339-12348.